1969

Magnetic coupling in composite ferromagnetic film structures

Jish-Min Wang
Iowa State University

MAGNETIC COUPLING IN COMPOSITE FERROMAGNETIC FILM STRUCTURES

by

Jish-Min Wang

A Dissertation Submitted to the

Graduate Faculty in Partial Fulfillment of

The Requirements for the Degree of

DOCTOR OF PHILOSOPHY

Major Subject: Electrical Engineering

Approved:

Signature was redacted for privacy.

In Charge of Major Work

Signature was redacted for privacy.

Head of Major Department

Signature was redacted for privacy.

Dean of Graduate College

Iowa State University
Ames, Iowa

1969

TABLE OF CONTENTS

I. INTRODUCTION

Much interest has been stimulated in studying thin magnetic films with uniaxial anisotropy since the first observation in 1955 by Blois (1). This has occurred partly because the desirable properties of a thin magnetic film provides a great potential application in high-speed, low-cost, large-capacity computer memories, and partly because the unique magnetic state of a thin film can serve as a powerful tool for studying basic magnetic properties of ferromagnetic materials. In the past decade, in particular, great effort in research and development has been made both in the area of basic material problems, such as, origins of anisotropy, mechanisms of coercivity and hysteresis, and mechanisms of magnetization reversal, etc., and in the area of thin film device applications, such as, techniques of utilizing thin magnetic films as computer memories, fabrication processes of memory arrays, interaction and disturb characteristics of storage elements in film memory arrays, and other related problems in device applications.

Special attention has been given in the past few years to possible techniques for improving the storage element disturb threshold which characterizes the stability of elements against disturbances existing in actual memory systems. The disturbances in thin magnetic film memory arrays are the results of the magnetic fields caused by currents in adjacent drive lines, dynamic or static stray field from the neighbor bits, eddy currents induced in conductors and ground planes, and currents contributed by the selection system. To be more specific, a storage element in a word-organized thin magnetic film memory system experiences

simultaneously a dc bit field in the easy direction from digit write currents, and an ac word field in the hard direction attributed to word lines in the neighborhood. As a result, after a period of time of operation, this particular stray field combination will cause reversal of the magnetization of this particular element through a slow domain wall motion process, the so-called domain-wall-creep (2), although the magnitude of the disturb field combination may be far smaller than the critical field for regular domain wall motion of the film elements. In other words, the disturb threshold of the film elements is reduced because of the presence of the domain wall creeping process.

Due to the presence of stray field disturbances in any practical film memory system, the achievable bit density of the array is then limited by the strength of the disturbing fields and the capacity of the film elements to withstand these fields. Consequently, it is apparent that measures of minimizing the existing disturbances and methods of improving the disturb thresholds of film elements become essential to obtaining high density, low cost memory arrays. Whereas the disturbances can be reduced by adopting a magnetostatically coupled second film and/or a ferrite keeper to achieve a semi-closed flux path (3), the disturb threshold of the storage elements can be improved by utilizing multilayer film structure of two identical permalloy layers each of 200Å to 300Å thick and separated by a thin non-magnetic metal layer (4-6).

Realizing the importance of developing a high-disturb-resist film element to materialize high-speed, low-cost, large-capacity thin magnetic film memory systems, the author initially intended to investigate the

creep characteristics of composite permalloy film structures. However, before the original goal was achieved, a very peculiar and interesting phenomenon, namely a magnetically alterable coercive force, was observed incidentally in the course of the investigation.

In the process of changing various parameters in order to optimize the disturb characteristics of the composite film, it was found that the top Ni-Fe film showed a rather high coercive force, typically about 20 Oe to 30 Oe, and a pronounced rotatable anisotropy field provided the film thickness was greater than a critical value of around 1700Å. The bottom Ni-Fe film of smaller thickness still showed a low coercive force, generally a few oersteds, and a normal uniaxial anisotropy field with highly rectangular hysteresis loop in the easy direction. It was observed in this particular composite film structure that the effective wall motion coercive force of the ordinary Ni-Fe (the bottom layer) could be changed by controlling the apparent easy direction (the direction of the remanent magnetization) of the anomalous Ni-Fe film (the top layer) provided the coupling between the two films was strong enough. To be more precise, the coercive force of the ordinary film had its highest value when the easy axes of the two coupled films were magnetically arranged to be parallel, and it had its lowest value when they were mutually perpendicular. A factor as large as five or six to one had been observed in the change of the coercive force of the ordinary film. Since the variation of coercive force could be done magnetically, the observed phenomenon was, thus, termed as the magnetically alterable coercive force phenomenon.

The author thus decided to concentrate his investigation on the magnetic coupling between the ordinary Ni-Fe film and the anomalous Ni-Fe film. In particular, the author studied the possible mechanisms contributing to the magnetically alterable coercive force observed in these particular composite film structures. Experimentally, measurements were made on the types of coupling and their magnitudes, the change of coercive force with various parameters, such as, the thickness of the ordinary films (i.e., the wall types of the ordinary films), the thickness of the intermediate layer (i.e., the strength of the coupling), and the angle between the two easy axes. Attempts were also made to obtain the Bitter patterns of the domain and the domain wall structures of the magnetic layers of the composite films. In addition, individual and composite film surface roughness were investigated by an electron microscope through the surface replica technique. Theoretically, the types and their effects were analyzed and the possible mechanisms contributing to the observed coercive force change were discussed. In particular, an analytical calculation, based on a simple configuration of the magnetization, was made on the magnetostatic interaction between different types of domain walls and the Bloch-wall-like stripes in the anomalous film. The effect of this interaction on the wall coercive force of the ordinary films was also calculated. A comparison between experimental results and the simple theory was made.

II. REVIEW OF LITERATURE

Great interest has been shown over the past few years in the problems of magnetic coupling between superimposed magnetic films. This interest is stimulated partly from the fact that coupled film structures provides an effective way of improving magnetic film properties with respect to computer memory applications (3-10), and partly from the potential application of localized domain wall interactions in composite film structures as large-capacity files (11). In general, the magnetic coupling observed in multilayer film structures with two or more magnetic films either in intimate contact or in sufficient proximity can be classified by its nature into two groups, namely the magnetostatic coupling and the exchange coupling.

According to the distribution of the magnetic poles attributed to the divergence of the magnetization, three different types of magnetostatic interaction have been observed in multilayer film structures. The most common one is the interaction of shape demagnetizing field associated with the magnetic poles at the film edges. This kind of interaction tends to align the magnetizations of each film in antiparallel direction to provide a close flux path for reducing the magnetic poles at the film edges. Consequently, the coupling becomes weaker as the film thickness (the magnetic poles) becomes smaller and as the film dimensions become large. Static and quasidynamic behaviors of magnetostatically coupled films have been studied by many workers (3, 12-15). Nondestructive readout (NDRO) thin film memories have been proposed by utilizing two magnetostatic coupled films with different coercive force

(14, 16), whereas destructive readout (DRO) film memories can be achieved by using two magnetic films of identical characteristics (3, 13, 15).

Wall-to-wall interaction, i.e., the interaction between the magnetic charge distribution attributed to the domain walls, is another type of magnetostatic coupling existing in composite film structures. The locked-in walls structure has been theoretically predicted as a direct result of the wall interaction by Fuller and Lakin (17), and experimentally observed by Puchalska and Spain (18), and by Biragnet et al. (19). Other effects of wall-to-wall interaction have also been studied by many researchers both theoretically and experimentally. Clow (20) observed that coercive force of laminated Ni-Fe films are greatly reduced because of the wall interaction. Domain wall structures under the influence of the interaction have been studied theoretically by many workers (5, 6, 21-26) and experimentally by others (7, 19, 27, 28). The coercive force of domain wall coupled with stripe-domain film has been reported by Sugita and Fujiwara (29) and Lo (30).

The third type of magnetostatic coupling is the interaction between dipoles created by the surface topography at the interfaces of the magnetic layer and the separation layer. This type of coupling is independent of the nature of the intermediate layers which can be insulators or nonmagnetic metals. However, the coupling is enhanced when the intermediate layer is a slowly evaporated metallic film in which granular structure usually formed. Depending upon the type of the interface topography and the thickness of the intermediate layer, the stable states of the magnetizations of the composite films are different. The magnetizations tend to align in parallel in the case of homogeneous

interface topography, such as, orange-skin interfaces (6, 31-32). Coupling energy of this type in the order of 0.01 erg/cm^2 has been theoretically calculated by Neel (32) for an orange-skin intermediate layer 100Å thick and an irregularity with 400Å in wavelength and 40Å in amplitude. On the other hand, the magnetizations tend to orientate in antiparallel if the interface topography is inhomogeneous, such as, interfaces of inland structures or columnar structures as observed in this study.

In general, the exchange coupling can be divided into positive coupling and negative coupling in the sense that, as the result of the coupling, the magnetizations in the two layer tend to orientate parallel or antiparallel, respectively. Whereas the positive exchange coupling can be observed in a composite film structure of two ferromagnetic films either in intimate contact (10, 33-36) or with thin separation (9, 37-39), the negative exchange coupling can only be found between a ferromagnetic film and an antiferromagnetic film in intimate contact (40, 41). The direct positive exchange coupling is the result of the direct exchange interaction between the magnetizations. The indirect positive exchange coupling is caused by the bulk diffusion of ferromagnetic atoms into the intermediate layer of Pd, or by the existence of magnetic bridges between the magnetic layers through pin holes and grain boundaries existing inside the intermediate layer of Au or Cr (37-38). On the other hand, the ferromagnetic-antiferromagnetic interaction at the interface is responsible for the negative exchange coupling observed in double layer structure such as, Gd-NiFe (40), Co-CoO, Ni-NiO and NiFe-NiFeMn, etc. (41).

The essential feature of the exchange-coupled films is that the magnetization everywhere in the films is subjected not only to the applied field, the anisotropy field and the magnetostatic fields, but also to the exchange interaction. As a consequence, the magnetization orientation in the film structure, generally, is nonuniform along the film thickness either in quiescent stable states or during switching. This, in turn, will substantially modify the usual uniaxial switching curves and effects the domain configuration of the composite film structure. The effects of the exchange coupling on domain wall structure have been studied rather extensively by Feldtkeller (5, 7) and his group (4, 6), and by the Grenoble group (19, 39). Meanwhile, the dynamic properties of exchange-coupled films have also been investigated both theoretically and experimentally by several groups of investigators (10, 33-36, 42-43).

III. EXPERIMENTAL INVESTIGATION

A. Materials and Fabrication of the Sample Films

The sample films used in this study were prepared by sequential vapor deposition of permalloy and chromium (sometimes gold was also used) by electron beam heating in the presence of a 80 Oe orientation field. In order to assure the mean free path of the vapor molecules in the atmosphere of the deposition chamber was longer than the source to substrate distance and to obtain consistent and repeatable results, the chamber pressure was kept below 5×10^{-5} torr during the entire deposition period.

The deposition station was a conventional vacuum system with a large glass bell jar (18 inches in diameter and about 30 inches in height). A mechanical pump was used to provide roughing and backing and an oil diffusion pump was installed to obtain a satisfactory vacuum for deposition. A water-cooled, mechanically rotatable table was so designed that several different materials could be evaporated sequentially with a single electron beam gun in one pumpdown. A mechanically rotatable shutter was also installed just below the substrate holder to minimize contamination during preheating of the sources. The rotatable shutter also provided a simple way of obtaining sample films of different thickness and/or different structure in one pumpdown by properly controlling its position during the deposition. Consequently, the uncertainties of evaporation conditions were virtually eliminated. In addition, the substrates were placed about 15 inches directly above the source to reduce the angle of incidence effects. Finally, a quartz crystal thickness monitor was

designed and installed to control the evaporation rates and to estimate the film thicknesses.

Corning cover glass was used as the substrate of this study mainly because its thermal expansion coefficient was very close to that of the permalloy and its surface condition, although not optically smooth, was satisfactory insofar as the smoothness was concerned. It is well known that the state of cleanliness of the substrates greatly influences the adhesion of the deposited films to the substrates and influences the magnetic properties of the permalloy films. The glass substrated were cleaned through the following procedure: (1) washed in a hot Alconox solution and then rinsed in flowing distilled water; (2) ultrasonically agitated in a clean Alconox solution for about 30 minutes and then rinse as before; (3) degreased in hot iso-propyl alcohol vapor for at least 30 minutes. This cleaning procedure produced a very consistent and satisfactory result.

Whereas permalloy of 81.7% Ni and 18.3% Fe was used for both magnetic layer in the composite film structure because of its near zero magnetostriction, chromium and gold were chosen as the intermediate materials because of their tendency to form granular structure at very slow evaporation rates. In order to obtain satisfactory evaporation rates, different containers were used for different materials. An alumina crucible wrapped with a thin tantalum strip was used for permalloy evaporation so that a deposition rate of about 20 to 30Å/sec was easily obtained. On the other hand, both chromium and gold were evaporated from tantalum boats placed directly on the water-cooled table. The typical

evaporation rates for the ordinary magnetic film, the anomalous magnetic film, and the non-magnetic metal film were about 20-30Å/sec, 10-20Å/sec and 1-5Å/sec, respectively.

Two evaporation sequences were performed to obtain sample films for different investigation. In one sequence of deposition, the ordinary Ni-Fe film with rectangular easy-axis loop was deposited first, then the separation layer of chromium (sometimes a very thin layer of gold was deposited just before the evaporation of chromium layer; however, later experiments showed that no significant effect on the magnetic properties of the composite films was induced by introducing the thin layer of gold). The anomalous Ni-Fe films with rotatable anisotropy was deposited last. This deposition sequence not only eliminated the possible effects of different substrate condition on the magnetic properties of the ordinary Ni-Fe film but also minimized the annealing effect on the anomalous film. (Later experiments showed that the magnetic properties were greatly influenced by the magnetic anneal.) The sample films thus obtained were used for magnetic properties measurements.

Another evaporation sequence was just the reverse order of the previous one, except a chromium layer of about 800Å was deposited before the actual sequence started, to provide a roughened substrate condition for the anomalous films. This set of test films was used for the Bitter-pattern study of the domain and domain wall structures of the ordinary films under the influence of the anomalous films.

According to the experimental observations, the critical thickness for the anomalous properties of permalloy film to prevail depended upon

the evaporation rates of the Ni-Fe film, the substrate temperature, the chamber pressure during evaporation, and particularly the evaporation rate of the intermediate layer. In general, the rougher the chromium (or gold) layer could provide, the thinner the critical thickness of the anomalous Ni-Fe film was. The typical critical thickness was about 1700Å under the following evaporation conditions: substrate temperature about 300°C, chamber pressure about 5×10^{-5} torr, deposition rates for chromium (or gold) and permalloy about 1-2Å/sec and 10Å/sec, respectively. Two different film thicknesses, say about 400Å and 1200Å, were chosen for the ordinary Ni-Fe films in order to be able to study the effects of different wall types under the influence of the anomalous film. The thickness of the separation layer varied from zero to about 500Å and the change of magnetic properties of the ordinary films could, then, be investigated as a function of the coupling. By the way, a test film was always deposited along with each deposition to provide a check for each separate film layer.

B. Electron-Microscope Study of Film Surface Roughness

Surface roughness attributed to each layer of the composite film structure was studied with the surface replica technique by means of an electron microscope. Evaporated carbon film replicas were used to improve the resolution. In addition, the carbon also served as a relief agent to prevent the adhesion of the plastic layer to the metal film surface. The possible artifacts caused by the stresses during the stripping process were greatly reduced by this procedure. Shadow casting with germanium was also employed to improve the contrast of the image and to enable to

measure the roughness of the surfaces.

On the film surface to be examined, a rather thick layer of three percent Formvar solution was coated, dried and then stripped to eliminate possible surface contamination. Afterward, a thin carbon film of about 50Å thick was vapor deposited on the specimen as surface replica. Then, a thin layer of one percent formvar solution was spread on the carbon-coated surface with an eyedropper, and the specimen was held at an angle to allow the solution to drain. When the Formvar film was thoroughly dried, it was scored at the thick end and moisture from the breath was condensed on the film. The moisture seemed to enter the film and facilitated separation of the plastic film with the carbon replica from the specimen. The plastic-film-backed carbon replica was then cut into small pieces and attached to copper grids, the sample holders for the electron microscope. At this stage, the replica was ready for shadow casting.

Germanium was chosen as shadow casting metal because of its relatively small granularity, ease of evaporation and particularly its high scattering power. It is known that too heavy a coating will obscure fine structures and too small a shadow angle will result in loss of detail behind projections. As a consequence, it is desirable to secure adequate contrast with the minimum thickness of deposit and at a moderate angle of shadowing. Shadow casting with 30Å germanium at 30 degrees shadow angle, as used throughout this study, showed good results. After shadow casting, the back up Formvar film was then dissolved away completely but slowly by placing the replica-loaded copper grids on a filter paper which was constantly wetted with ethylene dichloride.

After this dissolving process, these shadow-casted carbon replicas were then studied by means of an electron microscope.

The micrographs of the replicas indicated that shadow casting with germanium indeed effectively enhanced the visibility of the structure associated with surface elevations and depressions. The relatively sharp shadow resulted from the casting at a large distance provided a simple way of determining the height and the periodicity of the surface irregularity. By measuring the shadow length from the micrographs, the individual height of the surface elevations, could be estimated from the relation

$$h = d \tan \theta$$

in which h is the height of the surface elevation, d is the shadow length, and θ is the shadow angle. A schematic diagram of the shadow casting geometry was illustrated in Figure 1.

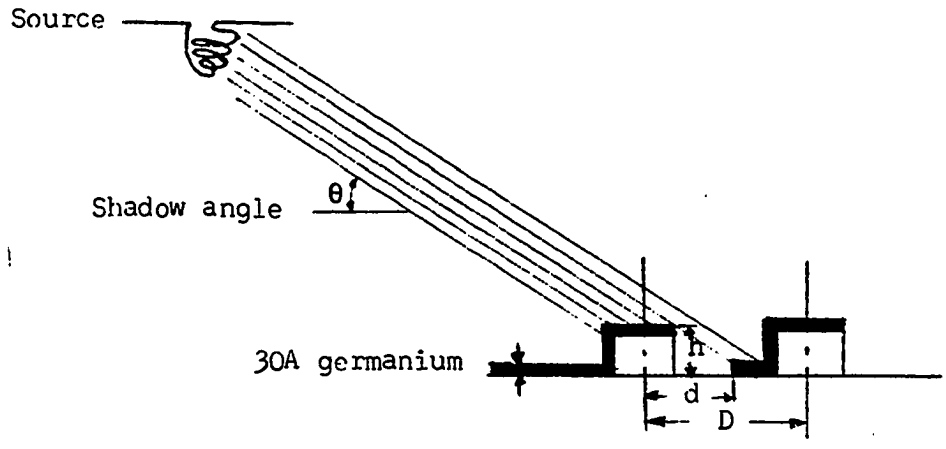

Figure 1. Schematic diagram of shadow casting geometry

One of the main findings in the micrographic study was that the surface roughness of the composite film structure was mainly attributed to the granular structure of the slowly evaporated intermediate metallic

layer. This finding was revealed from the observation that almost no granular structure was found in either single or double layer of permalloy films without metallic layer separation. On the other hand, rough surface was prevailed for films of chromium and gold and also the composite film structure of two Ni-Fe films separated by a thin layer of chromium or gold. Typically, the average heights, defined as the arithmetical mean of ten randomly selected elevations, were about 20-40Å and 200-350Å for permalloy films and chromium (or gold) films, respectively. The average periodicities, defined as the algebraic mean of ten randomly selected periods, were about 30-50Å and 250-400Å for magnetic and nonmagnetic films, respectively. Figure 2 showed the typical micrographs for different film structures.

Another significant observation of the study was the drastic change of the surface structure of the sample films subjected to magnetic anneal. Some of the composite film specimens were magnetically annealed in vacuum at about 350°C for at least two hours and remained in vacuum until the temperature dropped to room temperature. A magnetic field of about 80 Oe was applied during the entire process. After this annealing treatment, the anomalous properties disappeared. The surface structure showed local movement of atoms, particularly in the neighborhood of gross structure imperfections, such as, pin holes or grain boundaries, where both the mobility of atoms and the localized magnetic anisotropy were high. Consequently, a smoother surface was thus resulted. The change of the magnetic properties and the surface structures indicated that the anomalous properties of permalloy films were closely related to the rough surface topography attributed to the granular structure of the

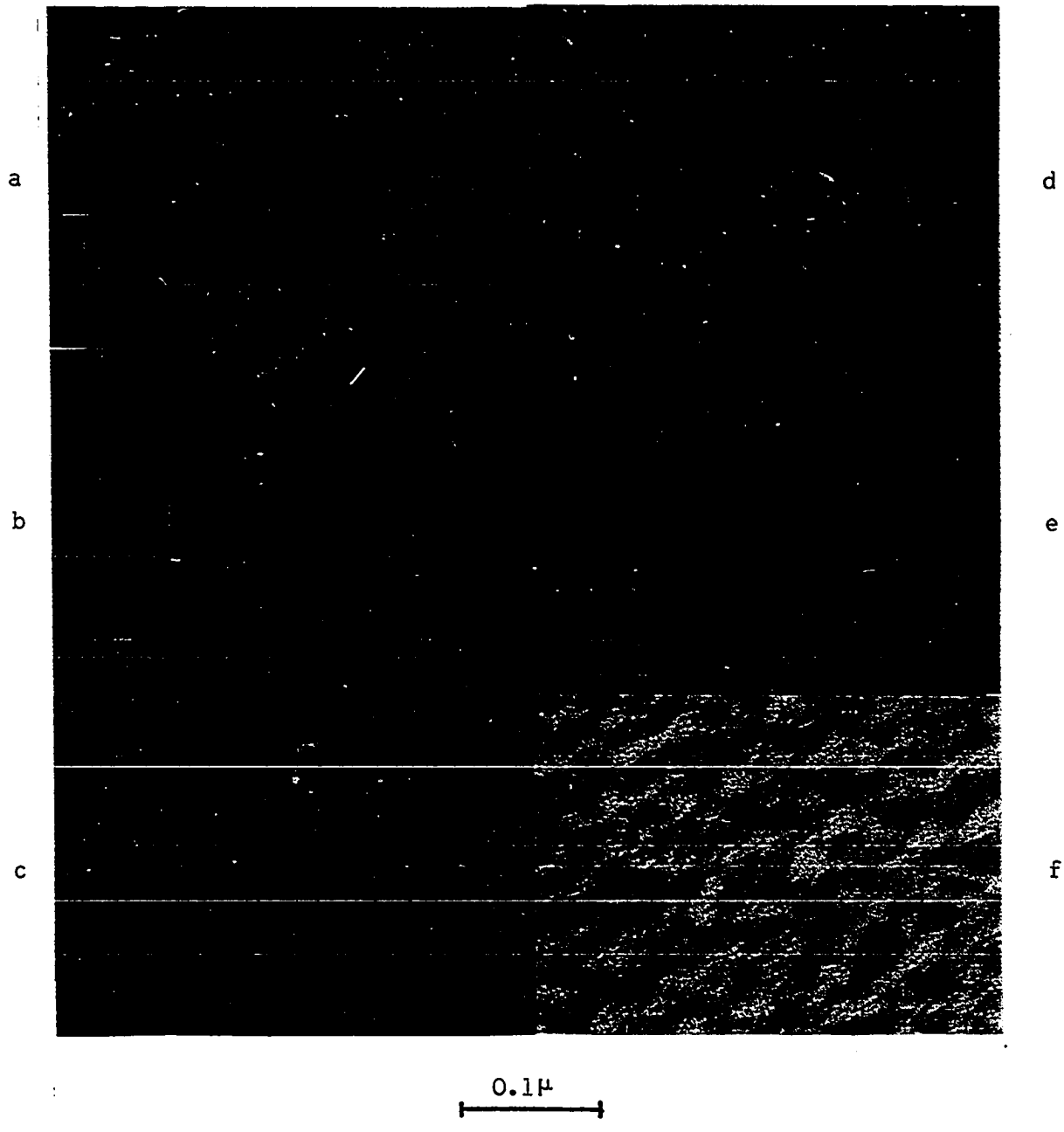

Figure 2. Electron micrographs of replicated film surface structures
(a) NiFe(1200A)
(b) NiFe(1200A)+NiFe(1700A)
(c) NiFe(1200A)+Cr(20A)
(d) NiFe(900A)+Cr(125A)+NiFe(900A)
(e) NiFe(1200A)+Au(11A)+Cr(13A)+NiFe(1700A)
(f) NiFe(1200A)+Au(11A)+Cr(39A)+NiFe(1700A)

intermediate layer. Figures 3 and 4, respectively, illustrated the change of magnetic properties and the change of surface condition of the composite film structure due to the magnetic anneal.

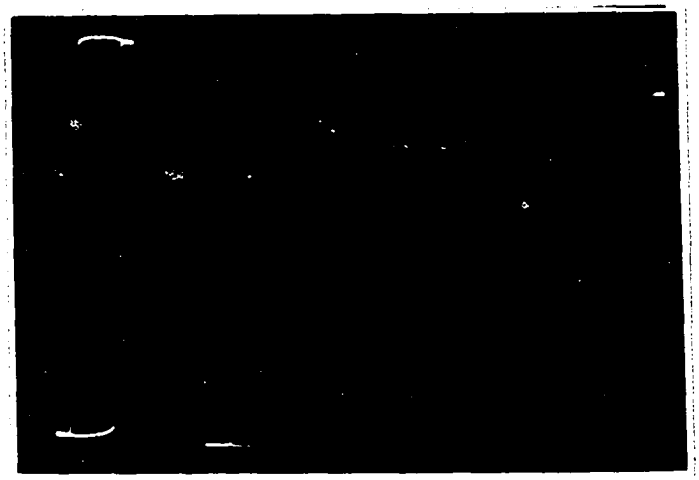

Figure 3. Hysteresis loops of the composite film structure before (right) and after (left) magnetic anneal

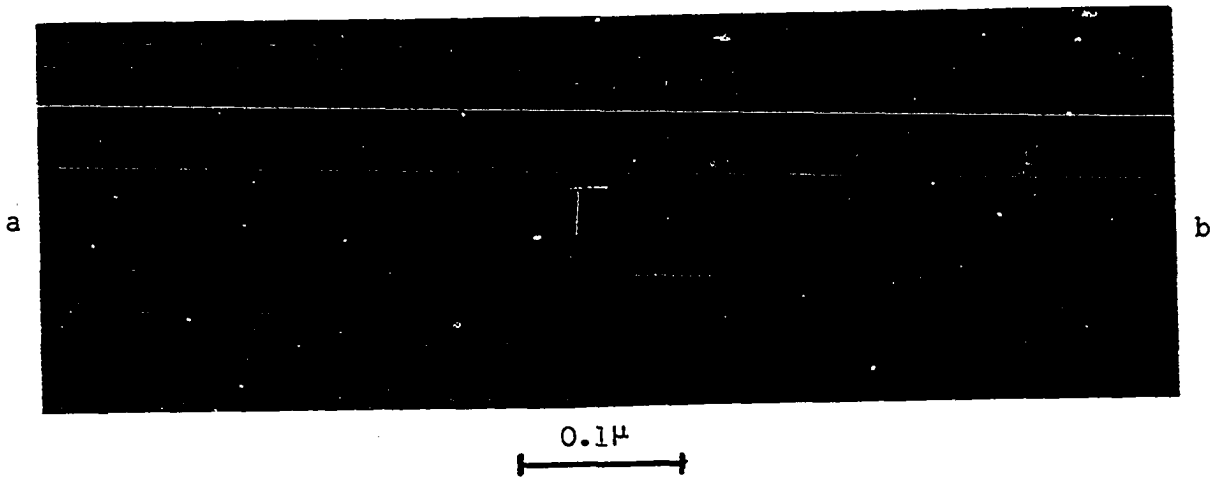

Figure 4. Electron micrographs of the composite film structure (a) before and (b) after magnetic anneal

C. Bitter-Pattern Study of Domain and Domain Wall Structures

In order to reveal the domain structure of the anomalous films and to demonstrate the effect of the coupling on the domain wall structures of the ordinary films, a study by means of Bitter powder pattern was attempted. A small drop of colloidal suspension of very fine magnetic particles (Fe_3O_4), the so-called Bitter solution, was placed on the film surface and formed into a thin layer by placing a clean microscope cover glass over the whole surface. Due to the ever present Brownian motion, the particles moved about in the suspension until they were captured by the magnetic stray fields associated with either the domain walls or the magnetic charge distribution attributed to the surface roughness. Consequently, the patterns formed by the captured particles represented the domain configurations of the specimen under the particular field condition, whereas the shapes of the lines formed by the captured particles showed the types of the domain wall structures. Thus formed patterns and line shapes were then studied by a metallurgical microscope with top field illumination.

Observations of most of the anomalous films showed mottled Bitter patterns (44). A close resemblance was noticed between the domain patterns and the surface topography of the film surface. This indicated that the magnetic stray field associated with the surface charge distribution attributed to the surface irregularity was the predominant factor in the formation of the domain patterns. However, some traces of fine domain structures, such as, stripe domains and ripple structures, were also observed is some portions of some of the test films. It was also interesting to note that normal walls revealed on the sample films

subjected to magnetic anneal. Figure 5 showed the domain patterns observed in the anomalous film before and after magnetic anneal.

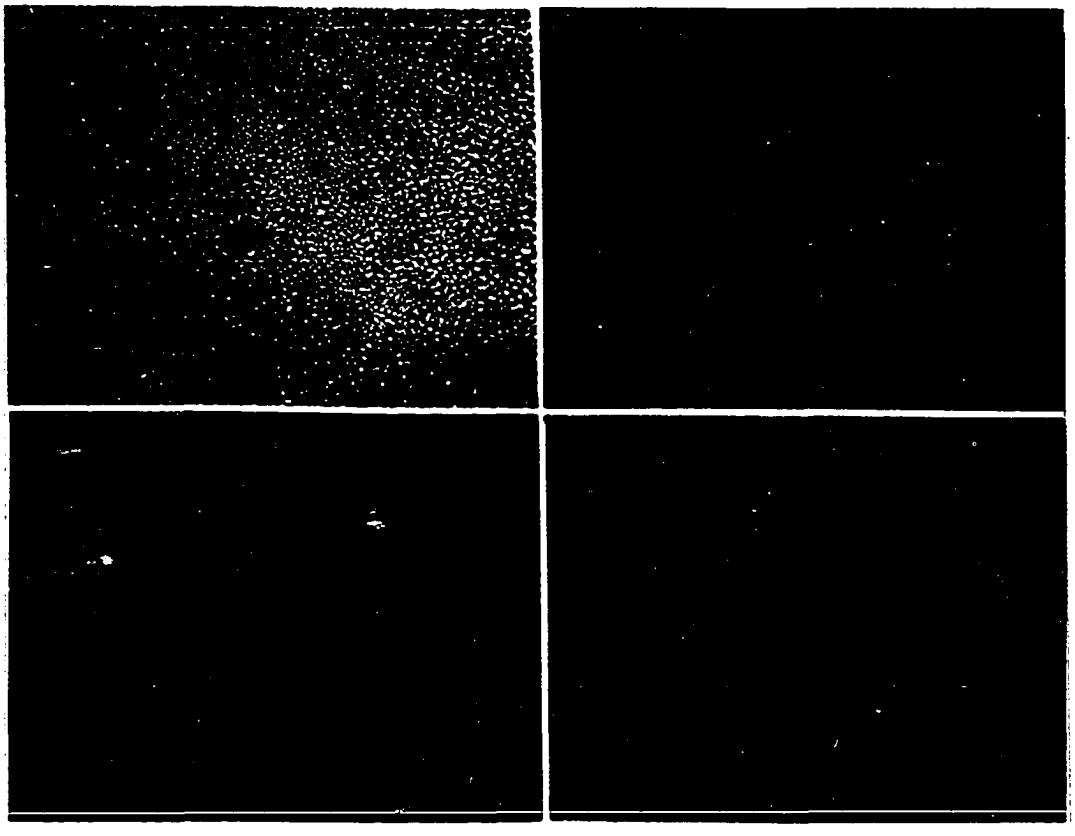

Figure 5. Domain patterns of the anomalous film before (a to c) and after (d) magnetic anneal

The domain wall structures of the ordinary films under the the influence of the anomalous films were also studied. The structural perturbation of walls of different wall spin configurations observed in the sample films clearly indicated the effect of the coupling. Figure 6 showed the perturbed wall patterns of the ordinary films of different thickness coupled with the anomalous films and the normal domain wall patterns of the corresponding single ordinary films.

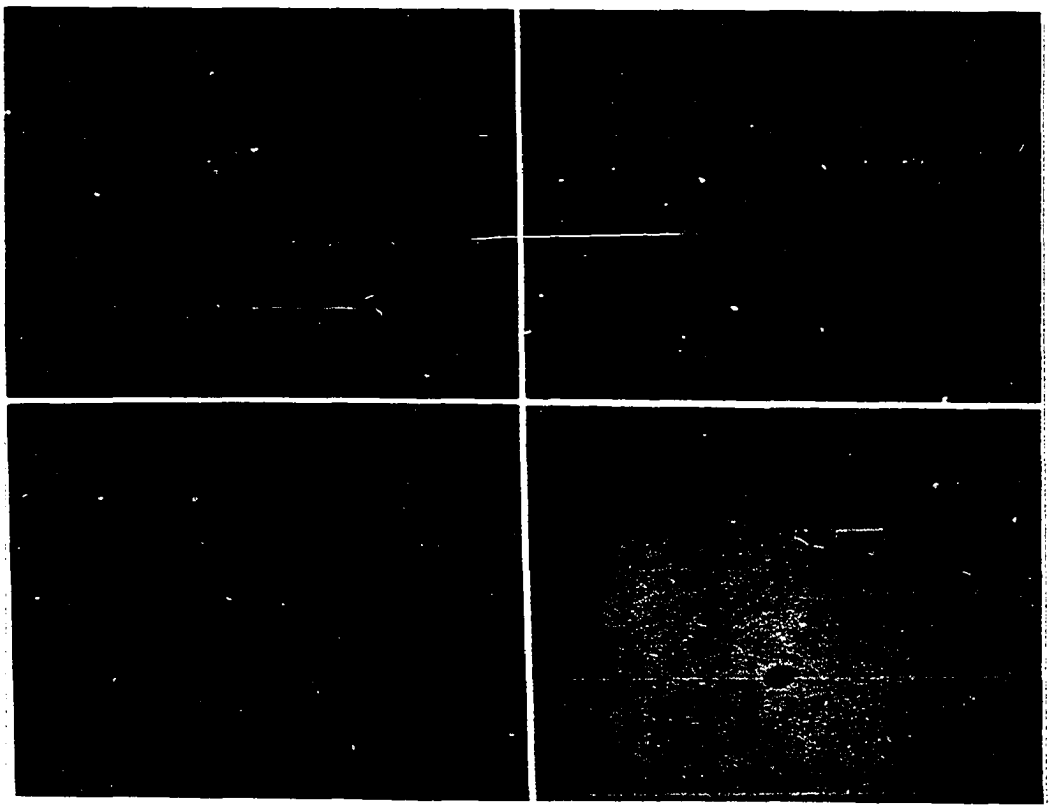

Figure 6. Domain wall patterns: (a) perturbed and (b) normal Neel walls; (c) perturbed and (d) normal Bloch walls

D. Techniques and Results of Measurements

All magnetic measurements were made by means of a conventional 60 cycle hysteresis loop tracer as sketched in Figure 7.

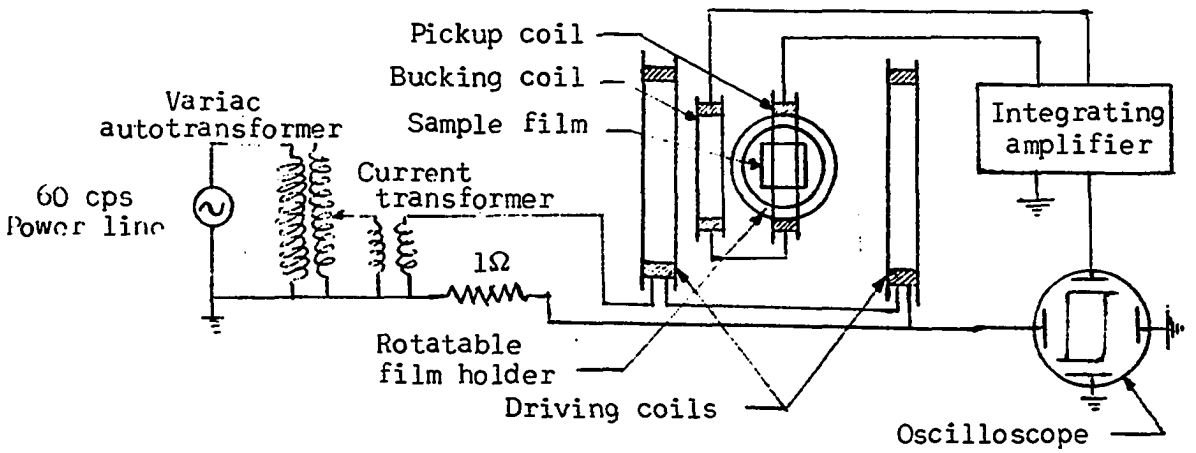

Figure 7. Schematic diagram of the hysteresis loop tracer

The driving field was applied by a pair of Helmholtz coils. The separation and the dimensions of the coils were designed to be almost equal to provide a very uniform field at the center of gravity of the coil pair. The film specimen was placed in a rotatable film holder and was then brought into a pickup coil. A bucking coil was also introduced and was connected to the pickup coil in such a way that the voltage induced by the air flux in the pickup coil was compensated. In addition, a movable aluminum sheet was also used to balance stray field disturbances by means of eddy currents induced in it.

The output of the pickup coil was fed to the input of the integrator whose output was then displayed as the vertical scale on the screen of the oscilloscope. This was proportional to the film magnetization parallel to the axis of the pickup coil, and could be used to check the film thickness if the scale was precalibrated by a sample film of known saturation magnetization and geometry. On the other hand, the horizontal scale, obtained from a one-ohm resistor in the driving field. Whereas the easy axis loop was used to measure the wall motion coercive force, the hard axis loop, particularly the initial slope at low transverse applied fields, was often used to measure the anisotropy field of the film.

1. Variation of coupling fields with intermediate layer thickness

The existence of the coupling between the magnetization of the ordinary film and the anomalous film was manifested experimentally by the presence of an effective coupling field which, in turn, was indicated by the easy-axis hysteresis loop displacement of the ordinary

film. In other words, when the easy axis of the ordinary film was arranged to be parallel to the apparent easy axis of the anomalous film by a permanent magnet or by a dc saturation field, the easy axis loop of the ordinary film exhibited a displacement attributed to the bias field caused by the anomalous film. Consequently, by observing the magnitude and the direction of the shifting of easy axis loop with respect to the magnetization direction of the anomalous film, the magnitude and the type of coupling could then be determined. However, this technique was valid only if the coupling fields and the coercive forces satisfied the relation

$$Hi' + Hi < Hc' - Hc$$

where Hi and Hi' are the coupling field acting on the ordinary film and the anomalous film, respectively, Hc and Hc' are the coercive force of the ordinary film and the anomalous film, respectively. Fortunately, the Hc' values (typically about 20-30 Oe) were much higher than the Hc values (generally under 10 Oe) in most of the composite films tested, the above relation was generally satisfied and the coupling fields, thus, could be measured. However, in the case of two extremely close-coupled films, the mutual coupling became so strong that the above relation was no longer valid; and the effective coercive force of both films became equal and no loop shifting could be observed. Figure 8 illustrated the technique for the measurement of coupling fields, whereas Figure 9 showed the hystersis loop under different bias field conditions.

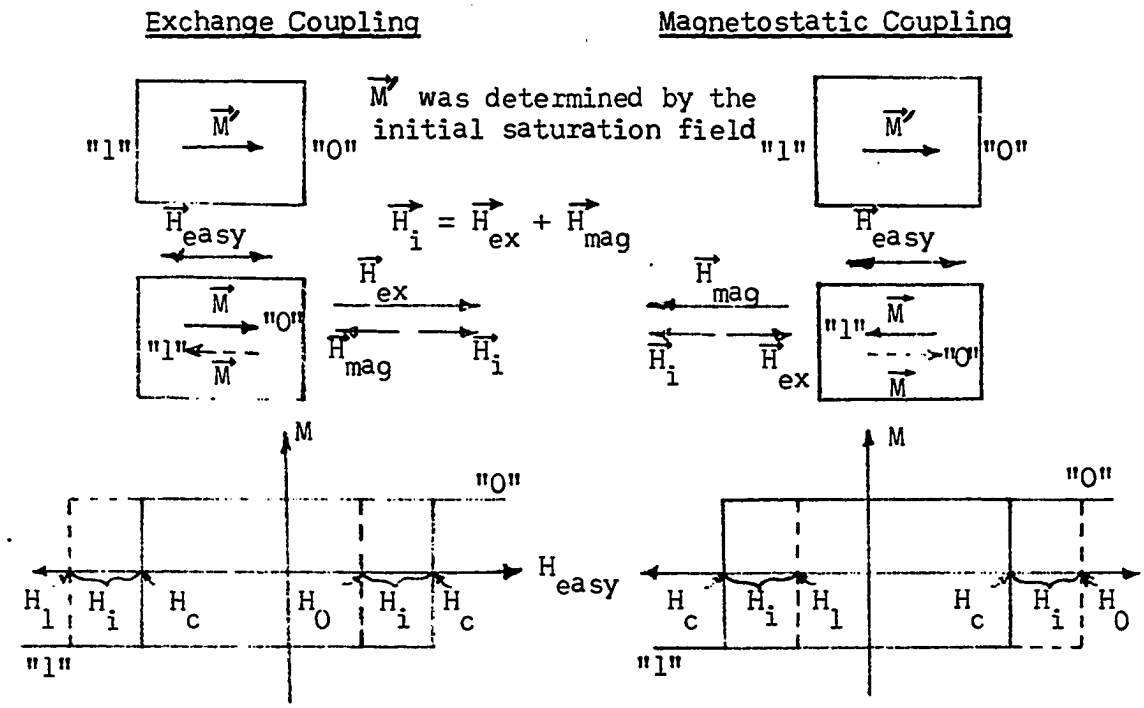

$$H_0 = H_c - H_i \qquad H_0 = H_c + H_i$$

$$H_1 = H_c + H_i \qquad H_1 = H_c - H_i$$

$$H_c = (H_0 + H_1)/2 \qquad H_c = (H_1 + H_0)/2$$

$$H_i = (H_1 - H_0)/2 \qquad H_i = (H_0 - H_1)/2$$

Figure 8. Method of measuring the coupling fields

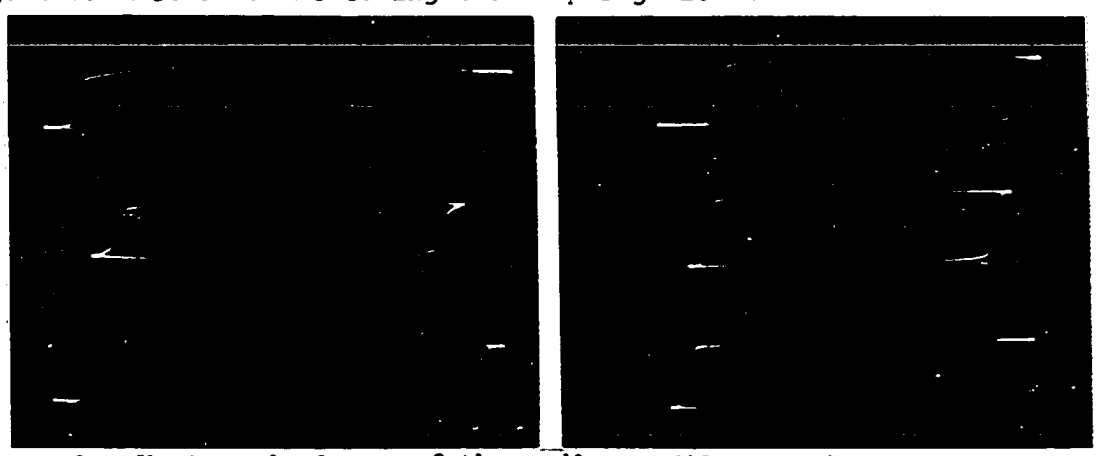

Figure 9. Hysteresis loops of the ordinary film: exchange coupling was predominant (left); magnetostatic coupling was predominant (right); in both cases, the anomalous film was in "0" state (top), demagnetized state (middle) and "1" state (bottom); horizontal scale: 5Oe/div. (left) and 2 Oe/div. (right)

The variation of the coupling field with the thickness of the intermediate layer, as shown in Figure 10, indicated two different types of coupling existed between the magnetizations when the anomalous film was saturated or nearly saturated. To be more precisive, the two films were exchange coupled when the intermediate layer thickness s was small, and became magnetostatically coupled as thickness s increased. The change was observed when the intermediate layer thickness was about 100Å and 200Å for the ordinary films of 400Å and 1200Å, respectively.

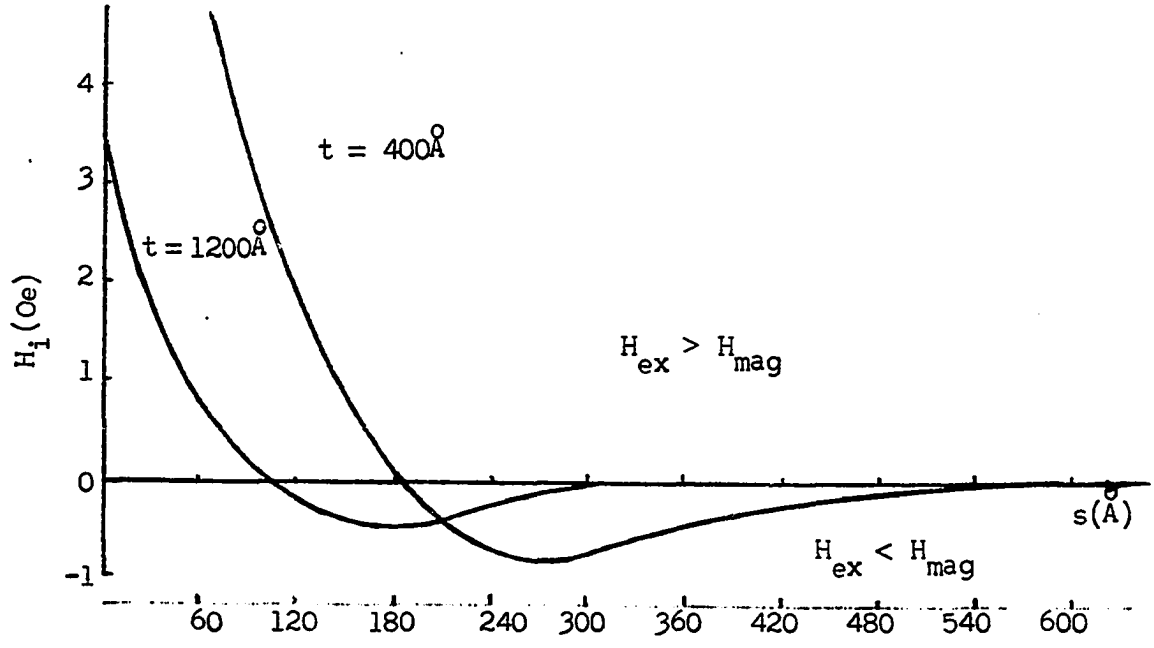

Figure 10. Variation of the coupling fields with the thickness of the intermediate layer s

2. Variation of coercive force with intermediate layer thickness

The magnetization reversal of a normal, uniaxial film by an easy axis applied field generally starts with the motion of domain walls associated with small regions of reversed magnetization at the film edge where the demagnetizing field is the strongest. As the applied field

increases, these reversed domains grow over the whole film, forming long walls parallel to the easy direction, and the reversal is then completed by a parallel shift of these walls. Because the field range in which this wall motion process takes place is very small so that the corresponding easy axis loop is highly rectangular. However, in the case of a composite film structure, the motion of domain walls in the ordinary film occurs only when the easy axis applied field exceeds the sum of the intrinsic wall coercivity and the coupling field attributed to the anomalous films.

Whereas the intrinsic wall coercivity of the ordinary film resulted from the film imperfections, such as, film thickness variation, localized anisotropy nonuniformity, inclusions, and substrate imperfection, etc., experimental evidence indicated that the main contribution of the coupling to the extrinsic wall coercive force came from the escape field attributed to the wall-to-wall interaction between the magnetic films. The extrinsic wall coercive force had almost the same values with or without observing easy axis loop shifting, i.e., with or without the presence of the bias field.

Figures 11 and 12 showed the variation of the effective wall coercive force of the ordinary film with the thickness of the intermediate layer. The results showed that the effective wall coercive force increased as a result of the interaction; and decreased exponentially as the intermediate layer thickness increased, then, finally leveled to its intrinsic value.

Figure 11. The dependence of the effective wall coercive force ($H_{cn} = H_{cni} + H_{cne}$) of the ordinary film of 400A thick on the intermediate layer thickness s

Figure 12. The dependence of the effective wall coercive force ($H_{cb} = H_{cbi} + H_{cbe}$) of the ordinary film of 1200A thick on the intermediate layer thickness s

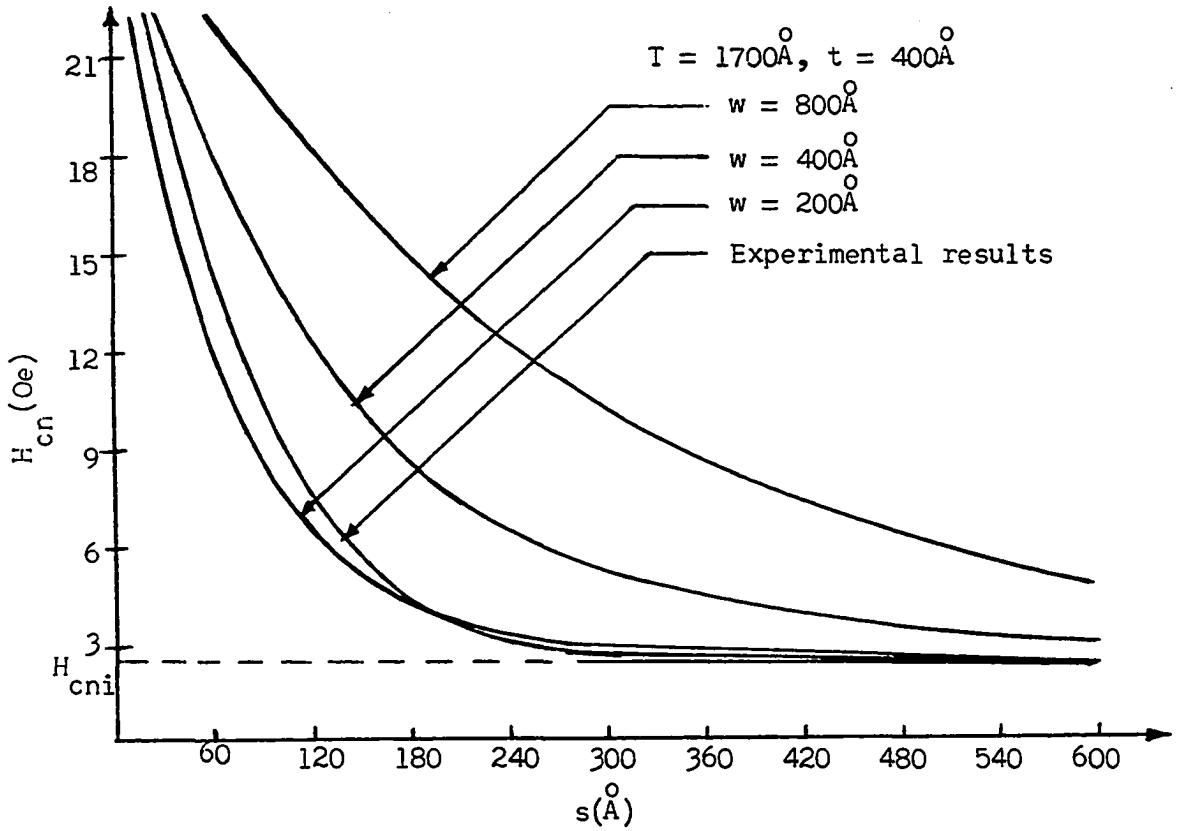
T = 1700Å, t = 400Å
w = 800Å
w = 400Å
w = 200Å
Experimental results
H_{cn} (Oe)
21
18
15
12
9
6
3
H_{cni}
60
120
180
240
300
360
420
480
540
600
s(Å)

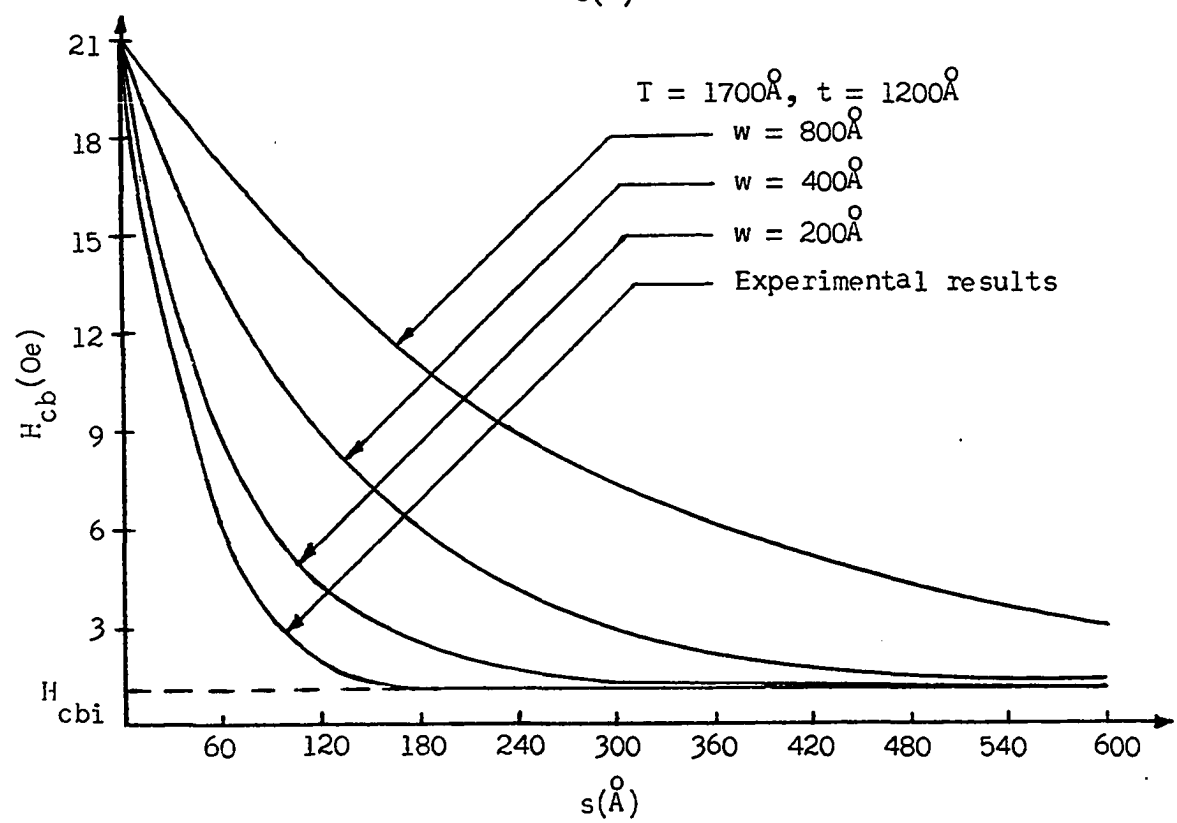
T = 1700Å, t = 1200Å
w = 800Å
w = 400Å
w = 200Å
Experimental results
H_{cb} (Oe)
21
18
15
12
9
6
3
H_{cbi}
60
120
180
240
300
360
420
480
540
600
s(Å)

3. Variation of coercive force with angle between the easy axes of the two magnetic films

One of the significant observations in the study was the dependence of the wall coercive force upon the angle between the easy axis of the ordinary film and the apparent easy axis (i.e., the direction of the remanent magnetization) of the anomalous film. When those two easy axes were magnetically arranged to be parallel, the wall coercive force of the ordinary films had the highest value. Whereas, the wall coercive force had the lowest value when the two easy axis were mutually perpendicular. The angular dependence of the wall coercive force, as shown in Figures 13 and 14, indicated that the stronger the coupling became (i.e., the thinner the intermediate layer thickness was), the larger the change of the coercive force was observed. The experimental data also showed that Neel type wall had a stronger angular dependence than Bloch type wall. The change of coercive force of the ordinary films of different thickness but with the same intermediate layer thickness was clearly illustrated by their corresponding easy axis loop, as shown in Figure 15.

Figure 13. The angular dependence of the effective wall coercive force of the ordinary film of 400A

Figure 14. The angular dependence of the effective wall coercive force of the ordinary film of 1200A

Figure 15. Easy-axis hysteresis loops demonstrate the angular dependence of the effective wall coercive force of the ordinary film of 400A (left) and 1200A (right) with same value of s; the upper traces are the loops when the axes are parallel and the lower traces are the loops when they are mutually perpendicular; Horizontal scale: 5 Oe/div. (left) and 2 Oe/div. (right)

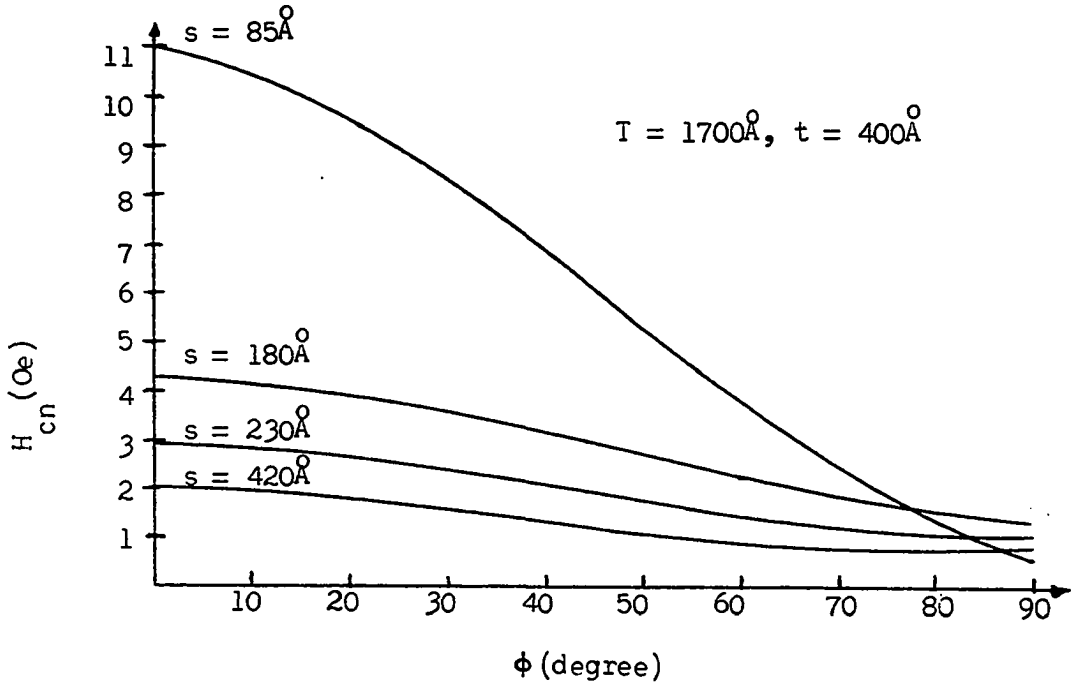
s = 85Å
T = 1700Å, t = 400Å
s = 180Å
s = 230Å
s = 420Å
H_{cn} (Oe)
11
10
9
8
7
6
5
4
3
2
1
10
20
30
40
50
60
70
80
90
ϕ (degree)

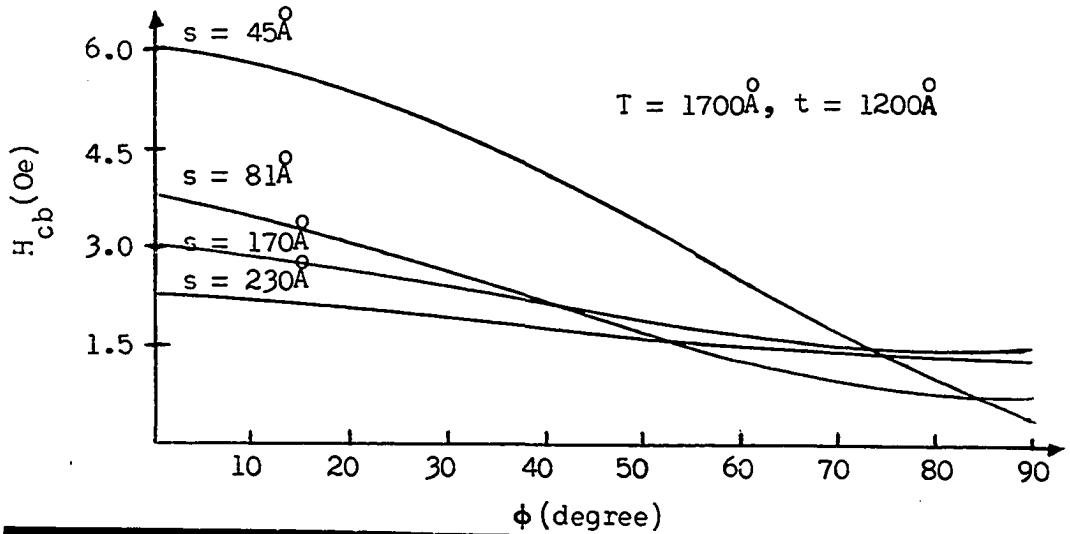
s = 45Å
T = 1700Å, t = 1200Å
s = 81Å
s = 170Å
s = 230Å
H_{cb} (Oe)
6.0
4.5
3.0
1.5
10
20
30
40
50
60
70
80
90
ϕ (degree)

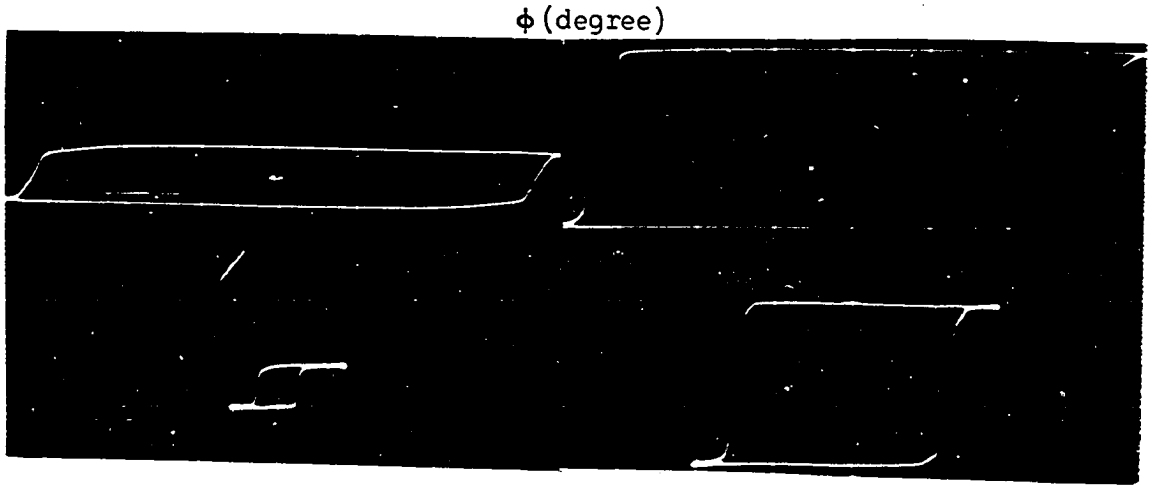

IV. THEORETICAL CONSIDERATION

A. Variation of Coupling Fields With Intermediate Layer Thickness

The experimental evidences indicates that there are two different types of magnetic coupling exist between the magnetization of the ordinary film and the anomalous film. When these two magnetic films are in sufficient proximity, the positive exchange coupling, resulted from the formation of magnetic bridges between the magnetic layers through pin holds and grain boundaries inside the chromium (or gold) layer (37-38), is predominant and the magnetizations tends to align in parallel. As the intermediate layer thickness increases, the positive exchange coupling becomes weaker and the longer-range magnetostatic coupling becomes prevalent. Consequently, the magnetizations tends to orientate in antiparallel. The change of the type of coupling is indicated by the change of the direction of easy axis loop shifting with respect to the same magnetization direction of the anomalous film.

According to the proposal by Bruyere et al. (9, 37), the effective exchange coupling fields Hi acting on the ordinary field can be related to the superficial energy of interaction Ei by the relation

$$Ei = -M\ Hi\ t\ \mathrm{Cos}\,\phi$$

where t is the thickness of the ordinary film, M is the saturation magnetization, and ϕ is the angle between the two magnetizations. They have also reported that the value of Ei is almost independent of t if thicker than 350Å. In other words, with all other film parameters being the same, the thinner ordinary film should have a larger coupling field and a greater transition thickness. The experimental results in this

study seems to be consistent with theirs.

Whereas the exchange coupling observed in the films tested is mainly indirect exchange interaction through the magnetic bridges, the magnetostatic coupling is largely contributed by the dipole-dipole interaction attributed to the surface charge distribution associated with the interface topographies with regard to the magnetic media. This is so because the shape demagnetizing field coupling is negligible in this case due to the extremely small separation-to-length ratio of the film specimen. The average demagnetizing field Hd in the films can be estimated by (13):

$$Hd \cong \frac{s}{b} Hs$$

where s is the intermediate layer thickness, b is the length of the film specimen, and Hs is the stray field at the film edges. Because the s/b value of the test film is about 10^{-6} to 10^{-7}, the coupling field of this type is generally smaller than 10^{-4} Oe and thus is insignificant insofar as the bias field is concerned. Meanwhile, the contribution of the wall-wall interaction is also immaterial because the bias field (i.e., the loop shifting) can be observed only when the anomalous film is saturated or nearly saturated (i.e., in remanent state).

Assuming an isotropic irregularity existed at each of the two interfaces between the magnetic film and the intermediate layer in a composite film structure, Neel (32) obtained a magnetostatic coupling energy of 0.01 erg/cm^2 for an intermediate layer of 100Å thick, and an irregularity with a wavelength of 400Å and an amplitude of 40Å. Although the shape of the interface topographies observed in this study may not be completely identical to Neel's assumption, the parameters of the irregularities are

in the same order of magnitude. Consequently, the coupling energy may have a similar value. In any case, the coupling field of this type should be predominant insofar as the contribution of the magnetostatic coupling to the bias field is concerned. Figure 16 illustrates the exaggerated film cross-section and the coupling field distributions in the composite film structures.

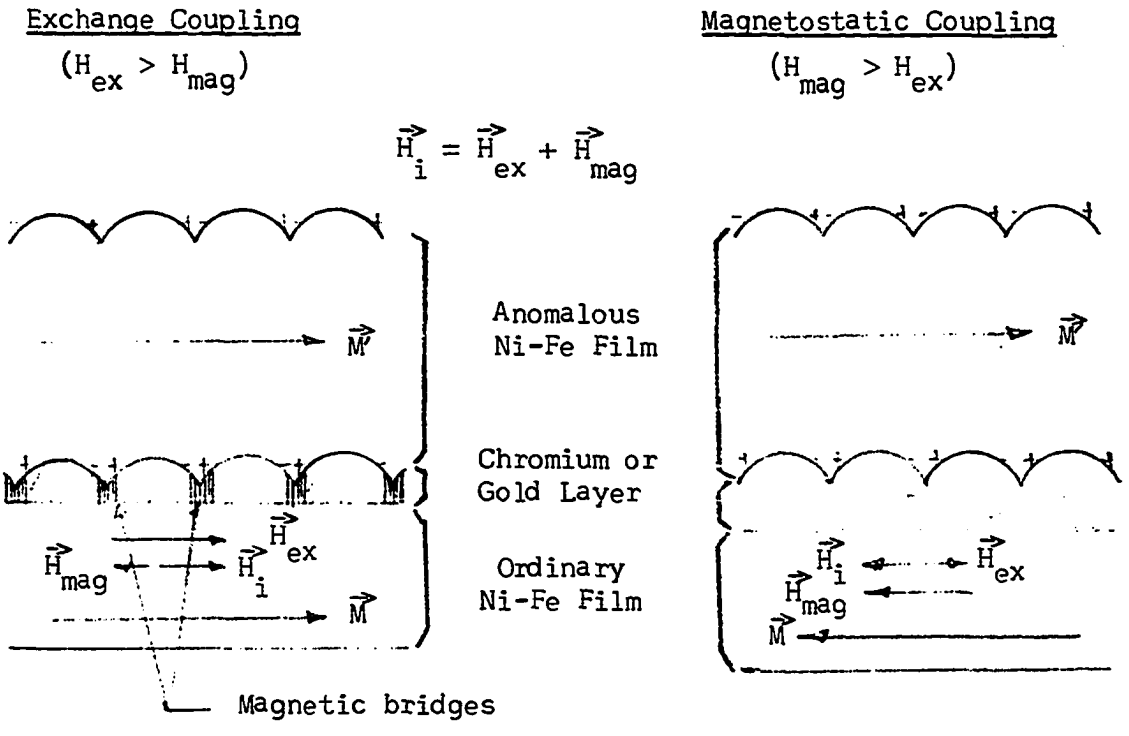

Figure 16. Coupling fields between the magnetizations of the composite permalloy film structure

B. Variation of Coercive Force With Intermediate Layer Thickness

Whereas the magnetic coupling between the magnetization of the two magnetic films produces a bias field as indicated by the ordinary films easy-axis loop shifting, the magnetostatic wall-to-wall interaction in the

films only greatly effects the effective wall coercive force of the ordinary film. As the experimental evidence indicates, the effective coercive force of the ordinary film in the composite film structure consists of two components: the intrinsic component originated from the film imperfections, such as, substrate surface roughness, film thickness variation, localized anisotropy variation, and inclusions etc.; the extrinsic component originated from the magnetostatic interaction between the normal wall and the Bloch-wall-like stripes on the anomalous film.

In contrast to the extrinsic component which diminishes as the interaction between the wall and the stripes vanishes, the intrinsic component remains about the same value as that of the single layer film. The intrinsic contribution to the wall coercive force has been extensively discussed elsewhere (45) and will not be repeated here. Instead, in this section an analytical calculation of the extrinsic contribution based on a simplified configuration is made.

As the experimental observation indicates, the value of the effective coercive force of the ordinary film is about the same whether the coupled anomalous film is in remanent state or in demagnetized state. In other words, the effective coercive force is not sensitive to the average magnetization or an antiparallel arrangement of the magnetization. Because of this insensitivity, the author decides to use the approach indicated in the following calculation for its relatively less mathematical complexity.

In the demagnetized state, the magnetization of the anomalous film is assumed to rotate helically about the x axis as illustrated in Figure 17. In other words, the angle θ between the magnetization and the +z direction

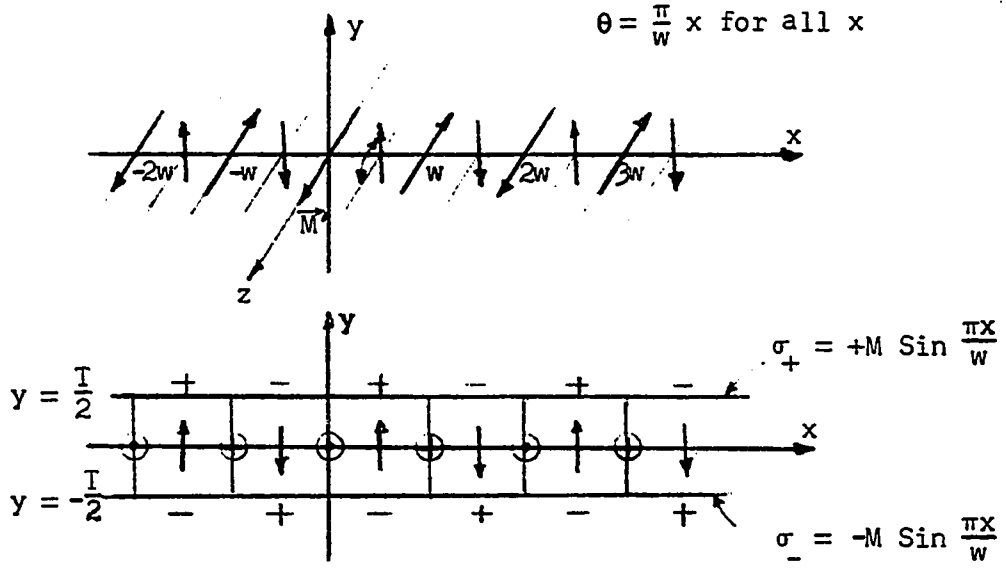

Figure 17. Schematic spin configuration of the magnetization of the anomalous film and the associated surface charge distribution

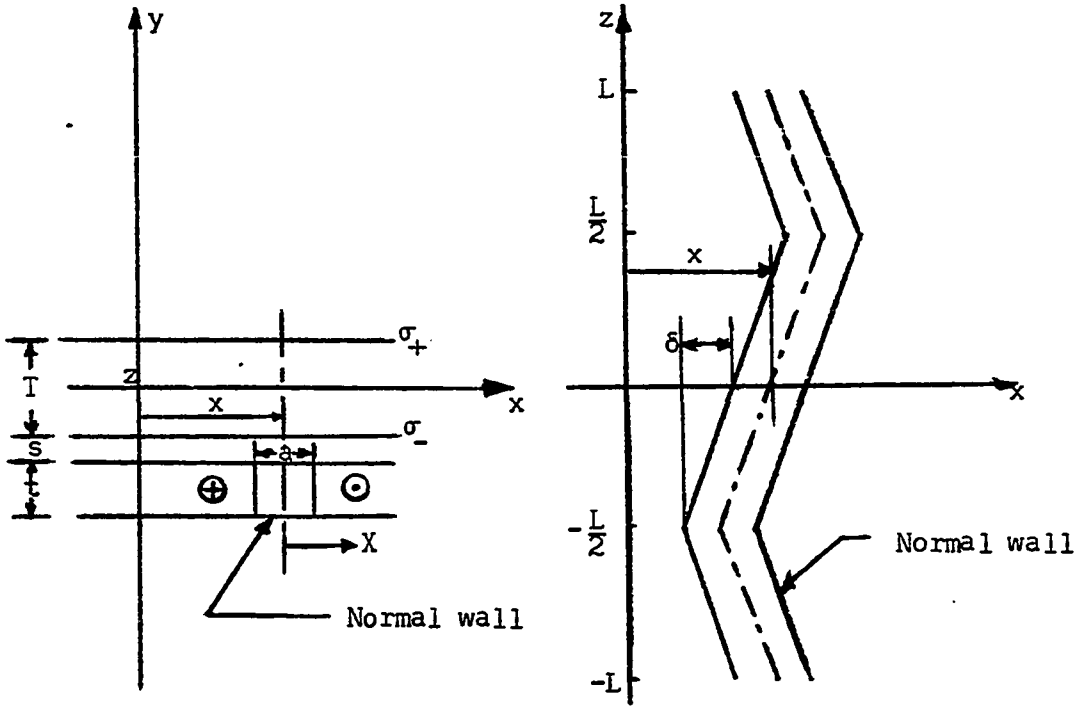

Figure 18. Coordinate system and the zigzag normal wall

(the apparent easy direction) can be expressed by:

$$\theta = \frac{\pi}{w} x \quad \text{for all } x \tag{1}$$

where w is the effective width of the stripe. This Bloch-wall-like spin configuration generates stripes of magnetic poles on the film surfaces. The surface density of the free poles on the upper and the lower surface, respectively, is given by $\sigma_+ = M \sin\theta$ and $\sigma_- = -M \sin\theta$, in which $M = |\vec{M}|$ is the saturation magnetization, and θ is given by Equation 1.

As indicated by the Bitter patterns, both the normal walls and the Bloch-wall-like stripes are wavy rather than straight lines in form. For simplicity, however, a regular zigzag one-dimensional normal wall 2L in wavelength and δ in amplitude, as shown in Figure 18, is assumed in the following calculation. The figure also shows the coordinate system for the composite film structure. In all cases, the y axis is chosen to be the film normal, while the xz plane divides the anomalous film into two identical portions. Let T, s, and t, respectively, be the thickness of the anomalous film (the top layer), the intermediate layer, and the ordinary film (the bottom layer). Then, the magnetostatic potential Φ_M associated with the surface charge stripes on the anomalous film surfaces is given by Equation A-6 in the Appendix.

1. Extrinsic coercive force of Neel walls

The magnetostatic interaction energy per unit wall length between a one-dimensional Neel wall in the ordinary film, as described by Equation A-14, and the Bloch-wall-like stripes in the anomalous film is given by Equation A-16:

$$E_{ne} = \frac{4M^2w^2}{\pi^2} \frac{\mathrm{Sin}(q\pi)}{q} \frac{\mathrm{Sin}(p\pi/2)}{(p - 1/p)} (1 - e^{-\frac{\pi T}{w}})(1 - e^{-\frac{\pi t}{w}})e^{-\frac{\pi s}{w}} \mathrm{Cos}(\frac{\pi}{w} x) \qquad (A\text{-}16)$$

where $p = \frac{a}{w}$, $q = \frac{\delta}{w}$.

Equation A-16 indicates that a moving Neel wall in the ordinary film is subjected to a periodically changing stray field attributed to the stripes on the anomalous film. Consequently, the effective wall coercivity is greatly effected. For a composite film structure, a wall motion in the ordinary film occurred only when the easy axis applied field is larger than the effective wall coercive force which is the sum of the intrinsic coercivity and the escape field associated with the interaction. Whereas the intrinsic wall coercivity is about constant, the extrinsic wall coercive force attributed to the interaction is given by:

$$H_{cne} = \frac{1}{2Mt} \left(\frac{dE_{ne}}{dx}\right)_{max}$$

Using Equation A-16, the final expression of H_{cne} is obtained:

$$H_{cne} = (\pm) \frac{2Mw}{\pi t} \frac{\mathrm{Sin}(q\pi)}{q} \frac{\mathrm{Sin}(p\pi/2)}{(p - 1/p)} (1 - e^{-\frac{\pi T}{w}})(1 - e^{-\frac{\pi t}{w}})e^{-\frac{\pi s}{w}} \qquad (2)$$

This equation shows that H_{cne} decreases exponentially as the intermediate layer thickness s increases and eventually vanishes. The parameter $q = \frac{\delta}{w}$ is so chosen that the value of the effective coercive force H_{cn} at $s = 0$ is equal to the corresponding value obtained from the experimental curve. Besides, the sign on the right hand side of Equation 2 is so chosen that the value of H_{cne} is always positive. The dependence of the effective coercive force ($H_{cn} = H_{cni} + H_{cne}$) on the intermediate layer thickness s is plotted in Figure 12 for several values of the effective stripe width w.

2. Extrinsic coercive force of Bloch walls

Following the same procedure just described, the extrinsic coercive force of one-dimensional Bloch walls is given by:

$$H_{cbe} = \frac{1}{2Mt} \left(\frac{dE_{be}}{dx}\right)_{max}$$

From Equation A-17, a similar expression for H_{cbe} is obtained:

$$H_{cbe} = (\pm) \frac{2Mw}{\pi t} \frac{Sin(q\pi)}{q} \frac{Cos(p\pi/2)}{(p - 1/p)} (1 - e^{-\frac{\pi I}{w}})(1 - e^{-\frac{\pi t}{w}}) e^{-\frac{\pi s}{w}} \qquad (3)$$

Equation 3 also shows that the extrinsic wall coercive force of the Bloch wall has the same dependence as that of the Neel wall on the intermediate layer thickness. The value of parameter q and the sign are also chosen in the same manner as that for the Neel wall. The dependence of the effective wall coercive of the Bloch wall is plotted in Figure 13.

C. Variation of Coercive Force With Angle Between the Easy Axes of the Two Magnetic Films

Both the experimental observation and the analytical calculation indicate that the main contribution of the effective wall coercive (more exactly the extrinsic wall coercivity) comes from the interaction between the wall and the surface charge distribution on the anomalous film surfaces. Consequently, if the easy axes are magnetically arranged to be in parallel, the normal wall moving in the ordinary film experiences a periodic-changed stray field attributed to the charge stripes on the surface of the anomalous film. As a result, the extrinsic wall coercivity increases and a higher effective wall coercive force is observed. However, as the angle between the easy axes increases, the interaction between the normal wall and the charge stripes decreases. Eventually, when the two

easy axes are mutually perpendicular, the interaction is virtually zero and the effective coercive force is about the intrinsic value.

In the case of pin hole or long range coupling, an additional contribution to the observation of the angular dependence of the wall coercive force is the angular dependence of the wall energy. This is revealed from the observation that the magnetic alterable coercive force phenomenon is more manifest when the anomalous film is the remanent state (i.e., when a bias field is present). Because of the presence of the bias field, the change of the remanent magnetization direction of the anomalous film causes the magnetization of the ordinary film turn away from the easy axis at equilibrium. The angle ξ between the equilibrant direction of the magnetization and the easy axis depends upon the strength of the bias field H_i and the angle ϕ between these two easy axes. Generally, the stronger the bias field H_i and the large the angle ϕ are, the larger the angle ξ becomes. Therefore, small angle rather than 180 degrees normal walls are usually resulted.

According to Middelhoek (45), the angular dependence of the Neel wall energy can be described by:

$$E_n = E_n(180) \left[1 - \text{Sin } \xi\right]^2 \tag{4}$$

and that of the Bloch wall by:

$$E_b = E_b(180) \text{ Cos}^2 \xi \tag{5}$$

in which $E_n(180)$ and $E_b(180)$ are the energy of the 180° Neel and the 180° Bloch wall, respectively; and ξ is the angle between the magnetization and the easy axis. From Equations 4 and 5, the coercive force of the small angle Neel walls is

$$H_{cn} = H_{cn}(180) \frac{(1 - \text{Sin } \xi)^{3/2}}{(1 + \text{Sin } \xi)^{1/2}} \tag{6}$$

and that of the small angle Bloch walls is

$$H_{cb} = H_{cb}(180) \text{ Cos } \xi \tag{7}$$

where $H_{cn}(180)$ and $H_{cb}(180)$ are the coercive force of the 180^{o} Neel wall and the 180^{o} Bloch wall, respectively. However, the angle ξ is always less than 90^{o}, the coercive force of the small angle walls, Neel walls or Bloch walls, is generally less than or equal to the value of the corresponding 180^{o} walls.

V. SUMMARY AND DISCUSSION

The main findings of the study are summarized and discussed as follows:

(1) The introduction of the chromium and/or gold intermediate layer is the key step of the study. Experimental evidence clearly indicates that the rough topographic structure of the intermediate layer is essential to the observation of the anomalous properties in the top permalloy layer of the composite film structure. It is believed that a large shape anisotropy as given by Equation A-10 is induced by the columnar structure resulted from the slowly evaporated chromium; and this is responsible for the existence of mottled Bitter patterns, low remanent magnetization, rotatable anisotropy, and the fine domain structures observed in the anomalous films (46-48).

(2) The existence of the film imperfections inside the intermediate layer, such as pin holes and grain boundaries, leads to the observation of the exchange coupling between the magnetization of the two magnetic films (37, 38). The dipole-dipole interaction, attributed to the surface charge distribution associated with the interface topography with respect to the magnetic media, is the main contribution to the observation of the magnetostatic coupling in the composite film structure. Both the exchange and the magnetostatic coupling produce a bias field as indicated by the easy-axis loop displacement of the ordinary film.

(3) The magnetostatic interaction between the wall in the ordinary film and the surface charge distribution on the anomalous film surface greatly affects the effective coercive force of the normal film.

Generally, the effective coercive force increases as the result of the interaction but decreases exponentially as the intermediate layer thickness increases. The experimental results and the analytical calculation based on a simple linear model, as described by Equations 2 and 3, match remarkably well for an effective stripe width of 200A which is smaller than the value estimated by the simple model. However, if a checker-board type surface charge distribution attributed to the mottled surface patterns or the wavy fine domain structures is used, as described in Section B of the Appendix, the discrepancy in the effective width can be greatly improved. For instance, if $w = m = 300\text{Å}$ (typical value of the periodicity of the surface irregularity) is used, the effective width is about 210Å, as calculated from Equation A-20.

(4) As the angle between the easy axes of the two magnetic films changes, both the interaction between the normal walls and the surface charge stripes and the angle between the magnetization of the ordinary film and its easy axis changes. Accordingly, the effective coercive force of the ordinary film is also changed. Therefore, it is believed that both the magnetic coupling between the magnetizations and the magnetostatic interaction between the wall of the ordinary film and the surface charge stripes on the anomalous film surface are responsible for the observation of the so-called magnetically alterable coercive force phenomenon.

VI. LITERATURE CITED

1. Blois, M. S., Jr. Preparation of thin magnetic films and their properties. J. Appl. Phys. 26:975-980. 1955.

2. Middelhoek, S. Domanenwandkriechen in dunnen Ni-Fe schichten. Z. Angew. Phys. 14:191-193. 1962.

3. Daughton, J. M. and Chang, H. Wall motion reversal in easy-axis-coupled films. J. Appl. Phys. 36:1123-1125. 1965.

4. Feldtkeller, E., Stein, K. U., and Harms, H. Improved magnetic film elements for memory applications. Proc. INTERMAG:8.4.1-8.4.6. 1964.

5. Feldtkeller, E. Wandbewegungsfeldstarken in magnetischen mehrfachschichten. Z. Angew. Phys. 18:532-534. 1965.

6. Feldtkeller, E., Fuch, E., and Liesk, W. Magnetostatische Koppling von domanen und von wanden in ferromagnetischen doppelschichten. Z. Angew. Phys. 18:370-373. 1965.

7. Feldtkeller, E. Coupled walls in multilayer films. J. Appl. Phys. 39:1181-1190. 1968.

8. Middelhoek, S. Properties of Ni-Fe double films. Z. Angew. Phys. 18:524-528. 1965.

9. Bruyere, J. C., Montmory, R., Massenet, O., and Neel, L. A coupling phenomenon between the magnetizations of two ferromagnetic thin films separated by a thin metallic film--application to magnetic memories. Proc. INTERMAG:16.1.1-16.1.4. 1964.

10. Lee, W. P. and Thompson, D. A. An exchange-coupled thin film memory device. IEEE Trans. Magnetics MAG-4:520-524. 1968.

11. Fuller, H. W. and Rubinstein, H. Methods of utilizing thin magnetic film properties for large-capacity files. In Yovits, M. C., ed. Large capacity memory techniques for computing systems. Pp. 163-176. New York, N.Y., Macmillan Co. 1962.

12. Chang, H. Analysis of static and quasidynamic behavior of magneto-statically coupled thin magnetic films. IBM J. Res. Dev. 6:419-429. 1962.

13. Chang, H., Yelon, A., and Voegeli, O. Internal field, dispersion, creeping, and switching speed of coupled films. J. Appl. Phys. 34: 1209-1210. 1963.

14. Oakland, L. J. and Rossing, T. D. Coincident current nondestructive readout from thin magnetic films. J. Appl. Phys. 30S:54-55. 1959.

15. Suits, J. C. and Pugh, E. W. Magnetooptically measured high-speed switching of sandwich thin film elements. J. Appl. Phys. 33S:1057-1058. 1962.

16. Pohm, A. V. and Mitchell, E. N. Magnetic film memories, a survey. IRE Trans. Electronic Computers EC9:308-314. 1960.

17. Fuller, H. W. and Lakin, L. R. Wall-wall interaction between thin magnetic films. J. Appl. Phys. 34:1069-1070. 1963.

18. Puchalska, I. B. and Spain, R. J. Interaction entre les parois magnetiques dans les couches minces superposees. Comptes Rendus 254:2937-2939. 1962.

19. Biragnet, F., Devenyi, J., Clerc, G., Massenet, O., Montmory, R., and Yelon, A. Interaction between domain walls in coupled films. Phys. Stat. Solidi 16:569-576. 1966.

20. Clow, H. Very low coercive force in nickel-iron films. Nature 194: 1035-1036. 1962.

21. Friedlander, F. J., Kneller, E., and Silva, L. F. Magnetostatic wall interaction effects in multilayer films. IEEE Trans. Magnetics MAG-1:251-254. 1965.

22. Friedlander, F. J. and Silva, L. F. On magnetostatic wall interaction effects in multilayer films. IEEE Trans. Magnetics MAG-2: 135-136. 1966.

23. Middelhoek, S. Domain wall structure in magnetic double films. J. Appl. Phys. 37:1276-1282. 1966.

24. Slonczewski, J. C. Theory of domain-wall structure in multiple magnetic films. IBM J. Res. Dev. 10:377-387. 1966.

25. Aharoni, A. Magnetostatically coupled Neel walls. J. Appl. Phys. 38:2252-2253. 1967.

26. Pisutova, N. Some pecularities of the behavior of domain walls in coupled thin Ni-Fe films. Z. Angew. Phys. 24:86-88. 1968.

27. Middelhoek, S. Perturbation walls in thin magnetic double permalloy films. Appl. Phys. Letters 5:70-72. 1964.

28. Friedlander, F. J. and Silva, L. F. Wall transitions in coupled films. J. Appl. Phys. 36:946-947. 1965.

29. Sugita, Y. and Fujiwara, H. Coercive force of thin magnetic films coupled with stripes domain Ni-Fe films. Appl. Phys. Letters 8: 73-74. 1966.

30. Lo, D. S. Magnetic properties of Ni-Fe films coupled with stripe-domain films. IEEE Trans. Magnetics MAG-4:721-722. 1968.

31. Neel, L. Sur un probleme de magnetostatique relatif a des couches minces ferromagnetiques. Comptes Rendus 255:1545-1550. 1962.

32. Neel, L. Sur un nouveau mode de couplage entre les aimantations de deux couches minces ferromagnetiques. Comptes Rendus 255:1676-1681. 1962.

33. Goto E., Hayashi, N., Miyashita, T., and Nakagawa, K. Magnetization and switching characteristics of composite thin magnetic films. J. Appl. Phys. 36:2951-2965. 1965.

34. Goto, E., Hayashi, N., Honma., Kuroda, R., and Miyashita, T. Switching characteristics of composite magnetic thin films. Japanese J. Appl. Phys. 4:712-720. 1965.

35. Siegle, W. T. Exchange coupling of uniaxial magnetic thin films. J. Appl. Phys. 36:1116-1117. 1965.

36. Thompson, D. A., Finzi, L. A., Change, H., and Albert, P. Magnetic film with helical anisotropy. J. Appl. Phys. 37:1274-1276. 1966.

37. Bruyere, J. C., Clerc G., Massenet O., Paccard, D., Montmory, R., Neel, L., Valin, J., and Yelon, A. Indirectly coupled films. IEEE Trans. Magnetics MAG-1:174-180. 1965.

38. Massenet, O., Briagnet, F., Juretschke, R., Montmory, R., and Yelon, A. Origin of coupling in multilayered films. IEEE Trans. Magnetics MAG-2:553-556. 1966.

39. Bruyere, J. C., Clerc, G., Massenet, O., Montmory, R., Neel, L., Paccard, D., and Yelon, A. Coupling effect between the magnetization of two thin layers separated by a thin nonmagnetic metallic layer. J. Appl. Phys. 36:944-945. 1965.

40. Hayashi, N., Goto, E., and Nishimoto, K. Antiparallel exchange coupling in Gd-permalloy composite films. Japanese J. Appl. Phys. 7:555. 1968.

41. Massenet, O. Coupling in multilayered magnetic films. IEEE Trans. Magnetics MAG-4:26-28. 1968.

42. Hayashi, N. Effective triaxial anisotropy in triple-layered thin magnetic films. Japanese J. Appl. Phys. 5:1148-1156. 1966.

43. Lin, Y. S. and Chang, H. Rigorous dynamic analysis of exchange-coupled film. J. Appl. Phys. 40:604-616. 1969.

44. Huber, E. E. and Smith, D. O. Properties of permalloy film having a magnetoelastic easy axis normal to the film. J. Appl. Phys. 30S: 267-269. 1959.

45. Middelhoek, S. Ferromagnetic domains in thin Ni-Fe films. Unpublished Ph.D. thesis. Amsterdam, the Netherlands, University of Amsterdam. 1961.

46. Lo, D. S. and Hanson, M. M. Origin of stripe domains in Ni-Fe films. J. Appl. Phys. 38:1342-1343. 1967.

47. Iwata, T., Prosen, R. J., and Gran, B. E. Perpendicular anisotropy in polycrystalline Ni-Fe thin films. J. Appl. Phys. 37:1285-1286. 1966.

48. Saito, N., Fujiwara, H., and Sugita, Y. A new type of magnetic domain structure in negative magnetostriction Ni-Fe films. J. Phys. Soc. (Japan) 19:1116-1125. 1964.

49. Neel, L. Energy of Bloch walls in thin films. Comptes Rendus, 241. Pp. 533-536. 1955.

VII. ACKNOWLEDGMENTS

The author wishes to express his deepest appreciation to his major professor, Dr. A. V. Pohm, for his constant guidance and many valuable discussions throughout the course of this study.

Gratitude is also due to Mr. J. Nissen for his help in constructing the quartz crystal thickness monitor and to Mr. T. Hamilton for the electron micrographs of the film surface structures. A special word of thanks is expressed to the Industrial Affiliate Solid State Electronics Program, the Engineering Research Institute at Iowa State University, and to the National Science Foundation for the financial support of the study.

Finally, the author also wishes to thank his wife, Sato, for her help in typing the first draft and for her remarkable patience and constant inspiration.

VIII. APPENDIX

A. Magnetostatic Interaction Energy Between a Normal Wall and the Bloch-Wall-Like Stripes

1. Magnetostatic potential attributed to the charge stripes

Maxwell's equations governing magnetostatics (electromagnetic units are used throughout this thesis) are:

$$\vec{\nabla} \times \vec{H} = 0 \tag{A-1}$$

and

$$\vec{\nabla} \cdot \vec{H} = -4\pi \vec{\nabla} \cdot \vec{M} \tag{A-2}$$

where $\vec{H}$ is the magnetic field and $\vec{M}$ is the magnetization. These equations show that $\vec{H}$ is derivable from a magnetostatic potential Φ_M, and that $-\vec{\nabla} \cdot \vec{M}$ acts as a magnetic charge density ρ_M. Thus, with $\vec{H} = -\vec{\nabla}\Phi_M$, Equation A-2 becomes

$$\nabla^2 \Phi_M = -4\pi \rho_M \tag{A-3}$$

However, according to the linear model of the spin configuration of magnetization of the anomalous film ($\theta = \frac{\pi}{w} x$, for all x, with w as the stripe width), the divergence of the magnetization $\vec{M}$ is zero everywhere in the film except at the film surface $y = \pm\frac{T}{2}$, where surface charges $\sigma_{\pm} = \pm M \sin(\frac{\pi x}{w})$ exists because of the discontinuity of the normal component of the magnetization. Therefore, the potential Φ_M in this case satisfies two-dimensional Laplace's equation (no z dependence)

$$\nabla^2 \Phi_M = \frac{\partial^2 \Phi_M}{\partial x^2} + \frac{\partial^2 \Phi_M}{\partial y^2} = 0 \tag{A-4}$$

Using the method of separation of variable and employing the following boundary conditions:

$$
\begin{aligned}
&(\bar{\Phi}_M)_{y=\frac{T}{2}+0} = (\bar{\Phi}_M)_{t=\frac{T}{2}-0} \\
&(\bar{\Phi}_M)_{y=\frac{-T}{2}+0} = (\Phi_M)_{y=\frac{-T}{2}-0} \\
&(\frac{\partial\bar{\Phi}_M}{\partial y})_{y=\frac{T}{2}+0} - (\frac{\partial\bar{\Phi}_M}{\partial y})_{y=\frac{T}{2}-0} = -4\pi M \sin(\frac{\pi x}{w}) \\
&(\frac{\partial\bar{\Phi}_M}{\partial y})_{y=\frac{-T}{2}+0} - (\frac{\partial\bar{\Phi}_M}{\partial y})_{y=\frac{-T}{2}-0} = 4\pi M \sin(\frac{\pi x}{w}) \\
&\bar{\Phi}_M(0,y) = \bar{\Phi}_M(x,0) = 0
\end{aligned}
\qquad \text{(A-5)}
$$

and

$$(\bar{\Phi}_M)_{y\to\infty} \text{ and } (\bar{\Phi}_M)_{y\to-\infty} \text{ are finite}$$

The final solution of Equation A-4 is obtained:

$$
\begin{aligned}
\bar{\Phi}_M(x,y) &= 4wM \sinh(\tfrac{\pi T}{2w}) e^{-\frac{\pi y}{w}} \sin(\tfrac{\pi x}{w}) \quad -\infty < x < \infty\,,\ \tfrac{T}{2} \le y < \infty \\
\bar{\Phi}_M(x,y) &= 4wM\, e^{-\frac{\pi T}{2w}} \sinh(\tfrac{\pi y}{w}) \sin(\tfrac{\pi x}{w}) \quad -\infty < x < \infty\,,\ -\tfrac{T}{2} \le y \le \tfrac{T}{2} \\
\bar{\Phi}_M(x,y) &= -4wM \sinh(\tfrac{\pi T}{2w})\, e^{\frac{\pi y}{w}} \sin(\tfrac{\pi x}{w}) \quad -\infty < x < \infty\,,\ -\infty < y \le -\tfrac{T}{2}
\end{aligned}
\qquad \text{(A-6)}
$$

2. Estimation of the stripe width w

The total free energy density E_T of the anomalous film under the assumed linear spin configuration of the magnetization is the sum of the demagnetizing energy E_S, the exchange energy E_A and the anisotropy energy E_K.

From Equation A-6, the magnetostatic potentials at the two film surfaces are:

$$
\begin{aligned}
&\bar{\Phi}_M(x,\tfrac{T}{2}) = 2wM(1 - e^{-\frac{\pi T}{w}}) \sin(\tfrac{\pi x}{w}) \\
&\text{and} \\
&\Phi_M(x,-\tfrac{T}{2}) = -2wM(1 - e^{-\frac{\pi T}{w}}) \sin(\tfrac{\pi x}{w})
\end{aligned}
\qquad \text{(A-7)}
$$

Then, the demagnetizing energy density E_S is given by

$$E_S = \frac{1}{2} \cdot \frac{1}{T} \cdot \frac{1}{2w} \int_{-w}^{w} \left[\Phi_M(x, \frac{T}{2}) \sigma_+ + \Phi_M(x, -\frac{T}{2}) \sigma_- \right] dx$$

$$= \frac{M^2 w}{T} \left(1 - e^{-\frac{\pi T}{w}}\right) \qquad \text{(A-8)}$$

If the exchange forces are assumed to act only between neighboring spins, then, the average exchange energy density E_A, associated with the model $\theta = \frac{\pi}{w} x$, can be roughly calculated:

$$E_A = \frac{1}{2w} \int_{-w}^{w} A \left(\frac{d\theta}{dx}\right)^2 dx = A \left(\frac{\pi}{w}\right)^2 \qquad \text{(A-9)}$$

where A is the exchange stiffness of the film, typically about 10^{-6} erg/cm.

Because of the formation of the columnar structure in the intermediate layer (eventually effecting the anomalous film also), a large value of shape anisotropy is induced in the film normal of the anomalous film. The shape anisotropy K_o can be estimated by (46, 47)

$$K_o \cong M^2 \frac{D^2}{(D + d)^2} \left[1 - \left(\frac{D}{D + d}\right)^2\right] \qquad \text{(A-10)}$$

In this equation M is the saturation magnetization, D is the columnar grain diameter, and d is the grain boundary layer width. Using $M = 800$ gauss, $D = 300\text{Å}$ (typical value obtained from the microscopy of the film) and $d = 50\text{Å}$ (estimated from the observed critical film thickness), the shape anisotropy, as given by Equation A-10, is about 4×10^5 erg/cm^3. This is about two order of magnitude large than the normal field induced anisotropy (generally about 10^3 erg/cm^3 for the permalloy used). Therefore, the average anisotropy energy density E_K is:

$$E_K = \frac{1}{2w}\int_{-w}^{w} K_o \cos^2\left(\frac{\pi}{w}x\right)dx = \frac{1}{2}K_o \qquad \text{(A-11)}$$

From Equations A-8, A-9 and A-11, the total free energy density is then

$$E_T = E_S + E_A + E_K$$
$$= \frac{M^2 w}{T}\left(1 - e^{-\frac{\pi T}{w}}\right) + A\left(\frac{\pi}{w}\right)^2 + \frac{1}{2}K_o \qquad \text{(A-12)}$$

If $T \gg w$ is assumed, then Equation A-12 becomes

$$E_T \cong \frac{M^2 w}{T} + A\left(\frac{\pi}{w}\right)^2 + \frac{1}{2}K_o$$

This energy is then minimized with respect to w:

$$\frac{dE_T}{dw} = \frac{M^2}{T} - \frac{2A\pi^2}{w^3} = 0$$

and the stripe width is obtained:

$$w = \sqrt[3]{\frac{2\pi^2 AT}{M^2}} \qquad \text{(A-13)}$$

Using M = 800 gauss, A = 10^{-6} erg/cm, T = 1700Å, the stripe width is about 800Å. For comparison, the corresponding value of w for small spin angle, as given by Saito et al. (48), is about 690Å. The insensitivity of the stripe width to the spin angle seems to confirm the observation of the insensitivity of the effective coercive force to magnetic state of the anomalous film.

3. Magnetostatic interaction energy between a one-dimensional Neel wall and the Bloch-wall-like stripes

For a one-dimensional Neel wall, the magnetization direction in the wall can be expressed by (49):

$$\phi = \frac{\pi}{a}X \quad \text{for} \quad -\frac{1}{2}a < X < \frac{1}{2}a \qquad \text{(A-14)}$$

where ϕ is the angle between the magnetization $\vec{M}$ and the +X direction, and a is the domain wall width. Then, the volume density ρ_M of the equivalent magnetic charge originated from the divergence of the magnetization is

$$\rho_M = -\vec{\nabla} \cdot \vec{M} = \frac{\pi}{a} M \, \mathrm{Sin}(\frac{\pi}{a} X) \qquad \text{(A-15)}$$

However, it is assumed that the magnetic charge density is not effected by the zigzag wall shape, as shown in Figure 18. Using Equation A-6 and A-15, the average interaction energy per unit length E_{ne} between the magnetic potential Φ_M and the magnetic charge density ρ_M can be calculated:

$$E_{ne} = \frac{1}{2L} \int_{-\frac{1}{2}a}^{\frac{1}{2}a} dX \int_{-(\frac{T}{2}+s+t)}^{-(\frac{T}{2}+s)} dy \int_{-L}^{L} dz \, \Phi_M \, \rho_M$$

$$= -\frac{2\pi w M^2}{aL} \mathrm{Sinh}(\frac{\pi T}{2w}) \int_{-(\frac{T}{2}+s+t)}^{-(\frac{T}{2}+s)} dy \, e^{\frac{\pi y}{w}} \int_{-\frac{a}{2}}^{\frac{a}{2}} dX \, \mathrm{Sin}(\frac{\pi}{a} X)$$

$$* \left[\int_{-L}^{-\frac{L}{2}} dz \, \mathrm{Sin} \frac{\pi}{w}(x + X - 2\delta \frac{L+z}{L}) + \int_{-\frac{L}{2}}^{0} dz \, \mathrm{Sin} \frac{\pi}{w}(x + X + 2\delta \frac{z}{L}) \right.$$

$$\left. + \int_{0}^{\frac{L}{2}} dz \, \mathrm{Sin} \frac{\pi}{w}(x + X + 2\delta \frac{z}{L}) + \int_{\frac{L}{2}}^{L} dz \, \mathrm{Sin} \frac{\pi}{w}(2 + X - 2\delta \frac{L-z}{L}) \right]$$

$$= \frac{4M^2 w^2}{\pi^2} \cdot \frac{\mathrm{Sin}(q\pi)}{q} \cdot \frac{\mathrm{Sin}(\frac{p\pi}{2})}{(p - \frac{1}{p})} (1 - e^{-\frac{\pi T}{w}})(1 - e^{-\frac{\pi t}{w}}) e^{-\frac{\pi s}{w}} \mathrm{Cos}(\frac{\pi}{w} x) \qquad \text{(A-16)}$$

where

$$p = \frac{a}{w}, \; q = \frac{\delta}{w}.$$

4. Magnetostatic interaction energy between a one-dimensional Bloch wall and the Bloch-wall-like stripes

The magnetization direction in a one-dimensional Bloch wall can also be described by Equation A-14 (49). However, ϕ, now, is the angle between the magnetization M and the +Y direction (the film normal). This spin configuration produces only a surface charge density of $\rho_+ = M \cos(\frac{\pi X}{w})$ and $\rho_- = -M \cos(\frac{\pi X}{w})$, respectively, on the surface at $y = -(\frac{T}{2} + s)$ and $y = -(\frac{T}{2} + s + t)$. Following the same procedure as before, the average interaction energy per unit length E_{be} between these surface poles and the potential Φ_M, as given by Equation A-4 is

$$E_{be} = \frac{1}{2L} \int_{-\frac{1}{2}a}^{\frac{1}{2}a} dX \int_{-L}^{L} dz \left[\rho_+ \Phi_M \Big|_{y = -(\frac{T}{2} + s)} + \rho_- \Phi_M \Big|_{y = -(\frac{T}{2} + s + t)} \right]$$

$$= \frac{4M^2 w^2}{\pi^2} \cdot \frac{\mathrm{Sin}(q\pi)}{q} \cdot \frac{\mathrm{Cos}(\frac{p\pi}{2})}{(p - \frac{1}{p})} (1 - e^{-\frac{\pi T}{w}})(1 - e^{-\frac{\pi t}{w}}) e^{-\frac{\pi s}{w}} \mathrm{Sin}(\frac{\pi}{w} x) \qquad \text{(A-17)}$$

B. Magnetostatic Potential of a Checkerboard Type Magnetic Surface Charge Distribution

As revealed by the Bitter patterns, the domain structures of the anomalous film either shows mottled patterns or wavy fine domains. For simplicity, a checkerboard type magnetic surface charge density of $\sigma_+ = +M \mathrm{Sin}(\frac{\pi x}{w}) \mathrm{Sin}(\frac{\pi z}{m})$ and $\sigma_- = -M \mathrm{Sin}(\frac{\pi x}{w}) \mathrm{Sin}(\frac{\pi z}{m})$ is assumed to exist on the film surface at $y = \frac{T}{2}$ and $y = -\frac{T}{2}$, respectively. In these relations, w and m are the half wavelength of the charge variation in x and z direction, respectively. Similar to the case of parallel charge stripes,

as described in the first part of the Appendix, the magnetostatic potential $\bar{\Phi}$, associated with the checkerboard surface charge distribution, satisfies three-dimensional Laplace's equation

$$\nabla^2\bar{\Phi} = \frac{\partial^2\bar{\Phi}}{\partial x^2} + \frac{\partial^2\bar{\Phi}}{\partial y^2} + \frac{\partial^2\bar{\Phi}}{\partial z^2} = 0 \qquad \text{(A-18)}$$

Again, using the separation of variable technique and employing the following boundary condition:

$$(\bar{\Phi})_{y = \frac{T}{2} + 0} = (\bar{\Phi})_{y = \frac{T}{2} - 0}$$

$$(\bar{\Phi})_{y = -\frac{T}{2} + 0} = (\bar{\Phi})_{y = -\frac{T}{2} - 0}$$

$$\left(\frac{\partial\bar{\Phi}}{\partial y}\right)_{y = \frac{T}{2} + 0} - \left(\frac{\partial\bar{\Phi}}{\partial y}\right)_{y = \frac{T}{2} - 0} = -4\pi M \sin\left(\frac{\pi x}{w}\right) \sin\left(\frac{\pi z}{m}\right) \qquad \text{(A-19)}$$

$$\left(\frac{\partial\bar{\Phi}}{\partial y}\right)_{y = -\frac{T}{2} + 0} - \left(\frac{\partial\bar{\Phi}}{\partial y}\right)_{y = -\frac{T}{2} - 0} = 4\pi M \sin\left(\frac{\pi x}{w}\right) \sin\left(\frac{\pi z}{w}\right)$$

$$(\bar{\Phi})_{x = 0} = (\bar{\Phi})_{y = 0} = (\bar{\Phi})_{z = 0} = 0$$

and

$$(\bar{\Phi})_{y \to \infty} \text{ and } (\bar{\Phi})_{y \to -\infty} \text{ are finite}$$

The final solution of Equation A-18 is obtained:

$$\bar{\Phi}(x,y,z) = \frac{4\pi M}{\lambda_y} \operatorname{Sinh}\left(\frac{\lambda_y T}{2}\right) \operatorname{Sin}(\lambda_x x) \operatorname{Sin}(\lambda_z z) e^{-\lambda_y y} \qquad \frac{T}{2} \le y < \infty$$

$$\bar{\Phi}(x,y,z) = \frac{4\pi M}{\lambda_y} e^{-\frac{\lambda_y T}{2}} \operatorname{Sin}(\lambda_x x) \operatorname{Sin}(\lambda_z z) \operatorname{Sinh}(\lambda_y y) \qquad -\frac{T}{2} \le y \le \frac{T}{2} \qquad \text{(A-20)}$$

$$\bar{\Phi}(x,y,z) = -\frac{4\pi M}{y} \operatorname{Sinh}\left(\frac{\lambda_y T}{2}\right) \operatorname{Sin}(\lambda_x x) \operatorname{Sin}(\lambda_z z) e^{\lambda_y y} \qquad -\infty < y < -\frac{T}{2}$$

where

$$\lambda_x = \frac{\pi}{w}, \ \lambda_z = \frac{\pi}{m}, \text{ and } \lambda_y = \sqrt{\lambda_x^2 + \lambda_y^2} = \frac{\pi}{w}\sqrt{1 + \left(\frac{w}{m}\right)^2}$$

From Equations A-6 and A-20, it is clear, then, that potential Φ decays faster than potential Φ_M in the film normal direction, if w in both cases has the same value. Consequently, the corresponding interaction energy also has stronger dependency on y.